NATIONAL AERONAUTICS AND SPACE ADMINISTRATION

Technical Report 32-1468

A Parametric Analysis of Venus Entry Heat-Shield Requirements

W. Jaworski

R. G. Nagler

JET PROPULSION LABORATORY

CALIFORNIA INSTITUTE OF TECHNOLOGY

PASADENA, CALIFORNIA

April 15, 1970

NATIONAL AERONAUTICS AND SPACE ADMINISTRATION

Technical Report 32-1468

A Parametric Analysis of Venus Entry Heat-Shield Requirements

W. Jaworski
R. G. Nagler

JET PROPULSION LABORATORY
CALIFORNIA INSTITUTE OF TECHNOLOGY
PASADENA, CALIFORNIA

April 15, 1970

Prepared Under Contract No. NAS 7-100
National Aeronautics and Space Administration

Preface

The work described in this report was performed by the Engineering Mechanics Division of the Jet Propulsion Laboratory.

Acknowledgment

The authors wish to thank J. M. Spiegel and F. Wolf of Jet Propulsion Laboratory for their assistance in performing heat-transfer and heating-uncertainty calculations. Also, the authors appreciate the help of B. Laub of Avco Space Systems Division in obtaining computer runs on heat-shield performance at very high entry velocities.

Contents

Contents (contd)

Tables

Figures

Contents (contd)

Figures (contd)

Abstract

A parametric study to determine heat-shield weight and thickness requirements for possible range of Venus entries is presented. The 1968 Venus (V-3) model atmosphere was used in calculating convective and radiative entry heating rates. The assumed trajectory matrix covers the entry velocity range of 32,000 to 44,000 ft/s. The lower velocity is representative of an out-of-orbit entry, and the higher velocity of an entry from a Venus–Mercury flyby.

A number of available heat-shield charring materials were considered. It was found that, subject to char shear-strength limitation, lower density materials are satisfactory for low energy entries; for higher energy entries, denser materials with chars of higher shear strength must be used.

A Parametric Analysis of Venus Entry Heat-Shield Requirements

I. Introduction

Differences in pressure–density profile, atmospheric gas composition, and scientific data requirements make Venus atmospheric entry missions considerably more complex than earth entry under equivalent velocity and ballistic-coefficient conditions. Venus entry vehicles, in at least the first generation, are envisioned to require deceleration at very high altitudes, materials with high thermal and mechanical efficiencies per unit weight, and resistance to high radiative heating rates. These initial requirements are further complicated by potential coupling effects caused by the preentry environments (e.g., ground handling, biological sterilization, launch pumpdown and vibration, and transit vacuum, radiation, temperature levels and gradients, and guidance engine vibrations). The specific effects of these preentry environments are discussed in more detail in Ref. 1.

Although the recent success of the Soviet Union in impacting three space probes on the surface of Venus has generated information indicating that life as we know it is unlikely on Venus, many other scientific questions concerning the planet and its relationship to the solar system remain unanswered. The continuing interest in atmospheric entry of Venus provides some impetus for the evolution of initial guidelines for the thermal protection of the scientific payload.

There are two major extremes in the possible design philosophies for choosing a thermal protection system for Venus entry. With minimal analysis, a heat shield can be designed and built and its reliability established through a suitable ground- or flight-based "proof test." In the other extreme, a comprehensive analysis can be made of all phenomena experienced during entry, and in this way, based on a parametric study of conservatively selected uncertainties, a heat-shield weight can be established. In this report, the full analysis option is explored in depth through a comprehensive parametric study of the heat-shield requirements. With this ability to analyze Venus entry, we can indicate the supplementary studies or tests that must be made to achieve a balance between reliability, weight, and cost values.

II. Mission Spectra

Numerous Venus entry missions have been studied in this country since 1963 (Refs. 2–10).[1] Each mission emphasized a particular Earth–Venus launch opportunity or a particular entry concept within an opportunity. As far as the entry portion of the mission is concerned, three major entry velocity ranges encompass all of the missions. Out-of-orbit missions tend to enter at approximately 32,000 ft/s; direct-entry missions, with or without a flyby, enter at 35,000–38,000 ft/s; and Venus–Mercury flyby missions, with a drop-off capsule, enter at 42,000–44,000 ft/s. Variations are envisioned with landers, buoyant stations, multiple probes, lifting bodies, pre-encounter propulsive deceleration, etc. To make this parametric study useful for the full spectrum of missions, entry velocities from 32,000 to 44,000 ft/s have been studied with numerous perturbations about the typical nominal trajectories for variations in entry angle, ballistic coefficient, size, and geometry.

III. Entry Conditions

The choice of a particular Venus entry trajectory will depend on many other factors besides heat-shield considerations. The foremost of these factors are the overall mission objectives and planning that generate basic entry-system requirements. These objectives may involve a number of possible alternatives relative to velocity and angles of entry for different types of payload. Consequently, the heat-shield requirements will vary with any combination of entry-trajectory parameters. To provide a useful range of information on entry heat shield, a matrix of entry trajectories was investigated.

A. Venus Atmosphere

The models of Venus atmosphere (Ref. 11) established on an interim basis in 1968 were reviewed for this study. These models, identified V-1 to V-6, were derived on the basis of flight information from *Mariner V* (U.S.A.) and *Venera 4* (U.S.S.R.) probes, and from supplemental radar information regarding the planet radius. The high density model V-3 has been selected as most probable, and the pertinent information on this atmosphere is:

(1) Planetary radius	6048 km
(2) Surface pressure	167 atm
(3) Surface temperature	770°K
(4) Cloud temperature	220–250°K
(5) Composition (vol %)	N_2 (10%), CO_2 (90%)
(6) Molecular mass	42.4 g/g-mole

The most important aspect of this atmosphere besides composition is its high temperature at the planet surface (1385°R). This temperature is higher than the bond-line (1060°R) and decomposition (1000–1400°R) temperatures of the high polymer resins that are the basic constituents of most presently available heat-shield materials. Thus, consideration of a prolonged descent and survival after landing should be regarded as a separate problem (Refs. 5 and 7).[2]

B. Shape Selection

The shape of a ballistic entry vehicle will significantly affect the thermal environment it will create on its way toward the planet surface. Such a shape must be carefully selected to give desirable dynamic characteristics and, at the same time, provide acceptable accommodation of aerodynamic heating caused by atmospheric braking.

The primary dynamic requirements are the stability of flight and the rate of deceleration. Stability of flight is necessary to prevent catastrophic failure as a result of tumbling. To maximize science output, however, deceleration should occur as early as possible in a low-density, upper atmosphere. For this reason the vehicle must have a very high drag coefficient C_D and a low weight per unit area.

The generally accepted entry-vehicle shape that reasonably fulfills the dynamic constraints described above, is a blunted cone with a half-cone angle and degree of bluntness suitably chosen to insure near optimum performance. For this study, a family of shapes having a 60-deg half-cone angle has been selected. The base diameter and nose radius (bluntness) of the cone are either kept constant or allowed to vary for assumed nominal entry trajectories. The 60-deg half-cone angle is

[1] Other pertinent studies are contained in the following Jet Propulsion Laboratory internal reports:

(1) Bourke, R. D., et al., *Feasibility Study of a 1970 Venus Capsule Mission*, Internal Report AS 760-6. July 1, 1967.

(2) Bourke, R. D., et al., *Study of a 1973 Venus Capsule–Lander Mission*, Internal Report AS 760-10. Sept. 15, 1967.

(3) Long, J. E., et al., *Study of a 1973 Venus–Mercury Mission With a Venus Entry Probe*, Internal Report AS 760-1. Aug. 18, 1967.

[2] Also see (2) of footnote 1.

favored at JPL because past studies have indicated that aeroshell-to-entry weight ratio generally decreases with increasing cone angle.

Several existing studies consider the range of half-cone angles between 30 and 60 deg, and indicate an optimum angle to be somewhere between 45 and 60 deg when both convective and radiative heating are considered (Refs. 5 and 7). To provide a comparison, 30- and 45-deg half-cone-angle blunted shapes were also investigated; the same base diameter and nose radius were used for each body.

Figure 1 presents an overlay sketch of three blunted cone shapes drawn to dimensions described in the preceding paragraph. By inspecting this drawing, one can conclude that the smaller the half-cone angle, the more difficult it is to accommodate a sizable payload while maintaining a low center of gravity, which is required for stability. Furthermore, the side surface covered by the heat shield increases considerably with a decrease in the half-cone angle. Another important observation is that the flow on conical surfaces of 45- and 30-deg half-cone-angle shapes is found to be turbulent during most of the entry, and this results in higher convective heating that in turn adversely affects the heat-shield performance.

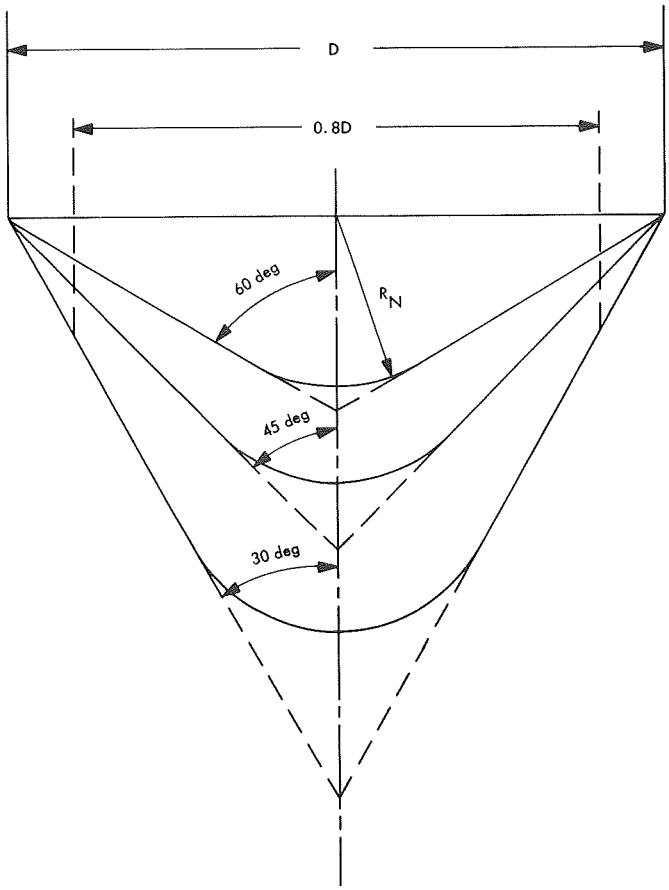

Fig. 1. Comparison of blunted-cone shapes

C. Thermochemistry Effects

The combustion process at an ablating surface is supported by the amount of free oxygen available in the boundary layer. The atmosphere of Venus does not appear to contain any free oxygen in its gas mixture; however, a certain amount of oxygen is freed by the dissociation of carbon dioxide at high temperatures in the shock layer in front of an entry vehicle.

To estimate the amount of available oxygen, a chemical equilibrium analysis was performed with the JPL Thermochemistry and Normal Shock Computer Program (Ref. 12). This program, in addition to quantizing various chemical species present at a given temperature and pressure, also computes the enthalpy of the gas.

The normalized enthalpy characteristics are given in Fig. 2 as a function of temperature for various pressure levels. The two parabolic curves, drawn by dashed line, represent the values used to obtain enthalpies at the wall; these enthalpies are needed for convective heat transfer calculations. Either set of values is used judiciously to approximate the actual temperature–pressure environment during entry along a specified trajectory. It is estimated that errors involved should be no greater than 10–15% at temperatures of 4000–7000°R. An average uncertainty of 10% is assumed for the entire trajectory. The appropriate parabolic equations representing each curve are also given in Fig. 2.

Figure 3 shows the amount of molecular and atomic oxygen that can be released during entry as a result of CO_2 dissociation and thermochemical recombination. These values are obtained along the lower enthalpy curve shown in Fig. 2; however, they are also satisfactory for the range of temperatures and pressures encountered in this study. Other oxygen species present, when added together, constitute a negligible amount.

Figure 4 includes the calculated weight fractions of available oxygen in the boundary layer as a function of temperature, based on the mole fractions indicated in Fig. 3. It is clear that up to 13% of oxygen is available at a temperature near 7000°R; however, a constant value of 10% is used in this analysis for a temperature range of 2000–7000°R.

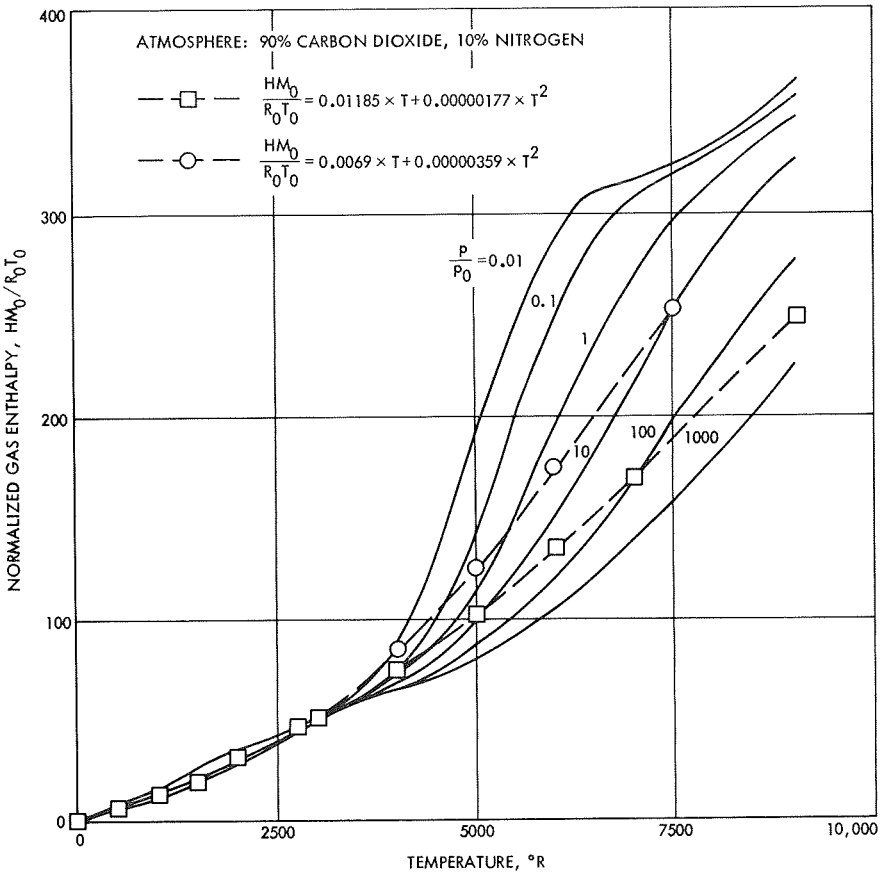

Fig. 2. Normalized gas enthalpy

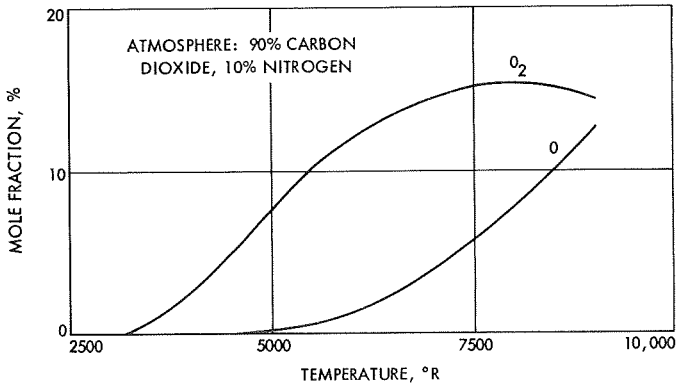

Fig. 3. Oxygen dissociated from carbon dioxide

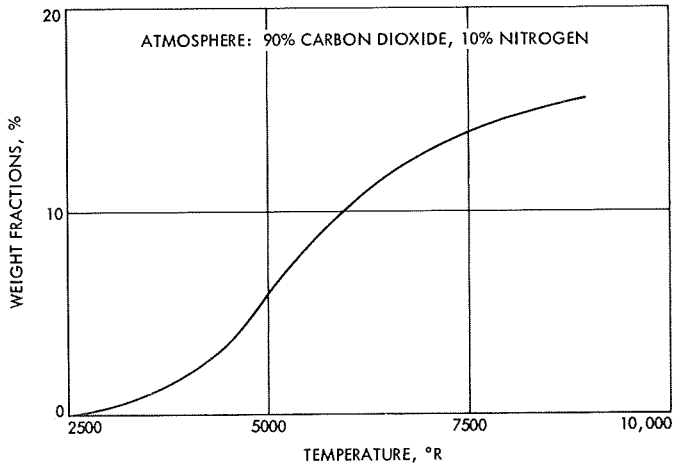

Fig. 4. Weight fractions of available oxygen

D. Selected Trajectory Matrix

The trajectory matrix selected for this study covers the entry velocity range from 32,000 to 44,000 ft/s to provide entry heating information for heat-shield performance calculations. Table 1 presents a complete matrix for 60-deg half-cone-angle shapes. This table contains the pertinent information required to obtain the trajectory computer runs. Entry velocity V_E and angle γ_E, ballistic coefficient M/C_DA, body diameter D, and nose radius R_N were the chief parameters varied. Nominal trajectories, for which variation of shape dimensions and material properties is made, are clearly marked.

For all runs, the spin rate P_E is assumed to be 1 rad/s and the angle of attack at entry α_E (approximately 1,000,000 ft from the planet surface) is held to -50 deg. These values of P_E and α_E were used because significantly higher magnitudes of either can result in excessive angles of attack near peak heating and loads for some capsule configurations. For example, analysis and test have shown that 60- and 45-deg half-cone-angle shapes have sufficient aerodynamic damping capability (with practical mass distributions) to lower the pitch oscillation to low angles by the time of peak heating if the initial angle of attack at entry is below -50 deg. Under higher initial angles of attack, the stagnation point is sometimes transferred to the outer edge of the capsule during significant portions of the heat pulse with subsequent potential for catastrophic failure.

Computer runs of trajectories for 45- and 30-deg half-cone-angle shapes were analyzed for the same nominal values shown in Table 1. However, as an indication of the basic trend, only 32,000 and 36,000 ft/s entry velocity cases were considered so that a comparison could be made with the heat-shield requirements for a 60-deg half-cone-angle entry vehicle.

E. Calculated Entry Conditions

The trajectory data have been obtained using a four-degree-of-freedom computer program (No. 1880) obtained on a contractual effort from Avco Corporation (Ref. 13). Extensive modifications, related primarily to radiative heating, were made by JPL and are described in Ref. 14. Another modification was introduced before the beginning of this study, namely the incorporation of radiative cooling by the method discussed in Ref. 15.

Computer runs have been made for the stagnation, junction, and shoulder points on the body. Junction means the line where the spherical and conical surfaces join together, and shoulder corresponds to the outer region of the cone, namely the area outside the 0.8 D (see Fig. 1). It will be observed that junction- and shoulder-trajectory data provide direct information on the radiative heating only. The convective heating, on the other hand, must be factored according to its known or assumed distribution along the body surface.

Figure 5 shows the laminar convective heat-flux distribution as a function of normalized distance from the stagnation point along the body contour, and Fig. 6 shows the appropriate pressure distribution as a function of normalized body radius. In the latter case, a dashed line approximation is used at the junction for half-cone angles of 60 and 45 deg. Although the pressure distribution shown in Fig. 6 is for specific flight velocity (36,243 ft/s), ambient density (4.3×10^{-6} slug/ft^3), and atmospheric composition (50% CO_2 and 50% N_2), it is believed that the data are reasonably valid for the range of conditions investigated in this study.

The trajectory program provides transition time from laminar to turbulent flow, and calculates the turbulent convective heat transfer at the sonic point. This information is used in the analysis to assess heat-shield performance in turbulent flow regions on the body. Finally, the flow-field enthalpy recovery for regions away from the stagnation points is calculated on the assumption of the isentropic expansion.

The heating rate–time histories of four nominal trajectories at 32,000, 36,000, 40,000, and 44,000 ft/s (see Table 1) are shown in Fig. 7. The solid and dotted lines represent convective and radiative heating rates, respectively. The 44,000-ft/s entry with peak radiative rates of the order of 13,500 Btu/ft^{2}s is certainly the most severe. The 40,000-ft/s trajectory represents an approximate ground simulation limit that is discussed in Section IV-A, and the 36,000-ft/s entry is typical of entry conditions well within present experience with earth reentry.

F. Evaluation of Heating Uncertainties

As it relates to atmospheric entry, the complex phenomena of heat transfer by convection and radiation to a body in the flow field can at best be only approximated analytically. The analytical results are then compared with experimental data to assess their accuracy. However, the accuracy of experiments, particularly on radiative heat transfer, is uncertain, and this fact makes it difficult to find a generalized point of departure or base line for the establishment of uncertainty criteria.

Table 1. Trajectory matrix[a]

Computer run	V_E, ft/s	M/C_DA, slug/ft^2	γ_E, deg	D, ft	R_N, in.	Remarks
1	32,000	0.3	−20	4	12	—
2			−45			—
3			−90			—
4		0.6	−20			—
5			−45			Nominal
6			−90			—
7		1.2	−20			—
8			−45			—
9			−90		12	—
10		0.6	−45	4	4	—
11				2	12	—
12				2	4	—
13				8	12	—
14			−45	8	4	—
15	36,000	0.3	−20	4	12	—
16			−45			—
17			−90			—
18		0.6	−20			—
19			−45			Nominal
20			−90			—
21		1.2	−20			—
22			−45			—
23			−90		12	—
24		0.6	−45	4	4	—
25				2	12	—
26				2	4	—
27				8	12	—
28			−45	8	4	—
29	44,000	0.3	−20	4	12	—
30			−45			—
31			−90			—
32		0.6	−20			—
33			−45			Nominal
34			−90			—
35		1.2	−20			—
36			−45			—
37			−90		12	—
38		0.6	−45	4	4	—
39				2	12	—
40				2	4	—
41				8	12	—
42			−45	8	4	—
43	40,000	0.6	−45	4	12	Nominal

[a] θ = 60 deg, P_E = 1 rad/s, α_E = −50 deg, C_D = 1.528.

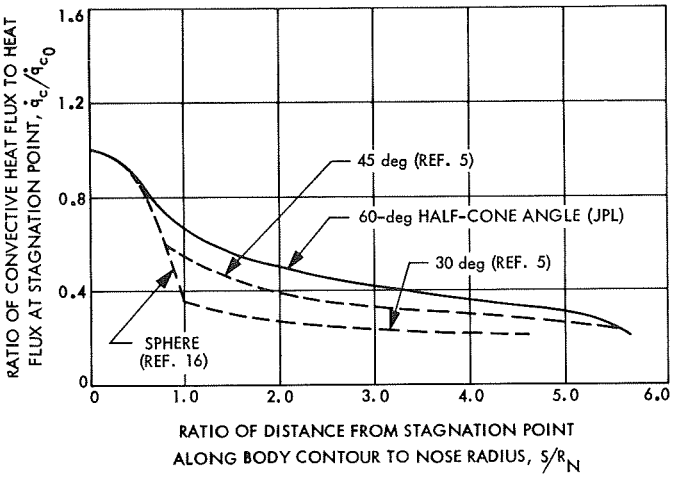

Fig. 5. Distribution of laminar convective heat transfer on a sphere-cone shape

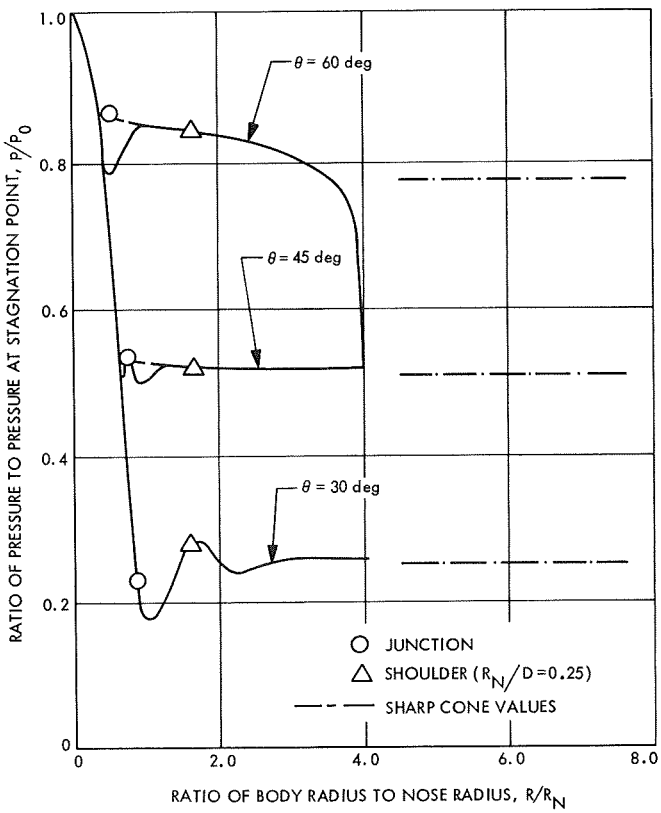

Fig. 6. Distribution of pressure on a blunt body

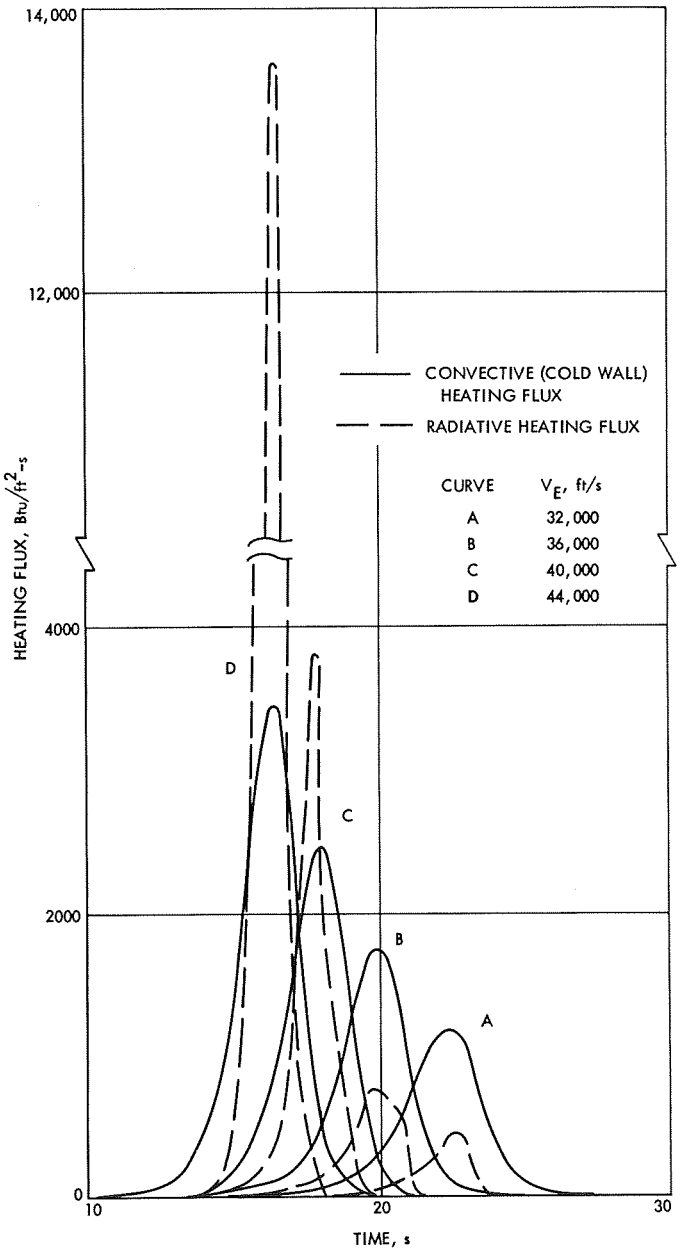

Fig. 7. Convective and radiative heating fluxes for nominal entry trajectories

In this analysis, the assumed base line is the computer program output. This output is compared with the available dispersion band of experimental points, and thus the deviation of analytical results from most credible experimental values is assessed. Clearly, the uncertainty factor applied in this manner represents a relative value. If a different computer program were used to obtain heat transfer data, correction would have to be made for disparity in outputs.

Figure 8 indicates the amounts in percent by which the stagnation point convective heating could be underestimated in the present analysis. These data are presented as a function of flight velocity. The point of maximum heat flux, approximately 0.85 V_E, is used for selection of the appropriate uncertainty factor. The work described in Ref. 17 formed the basis for arriving at the uncertainty values. The estimated uncertainties in heat-flux distribution are shown in Fig. 9. These uncertainties should be considered with those of the stagnation point. The calculated turbulent convective heating should be within 20%, and this is the only factor applied in calculating maximum possible heat transfer in the turbulent flow region.

Validation of the shock layer radiative heat transfer predictions used in the 1880 computer program for a 90% CO_2 and 10% N_2 gas mixture is difficult because the accurate experimental data are unavailable. However, use of existing information for equilibrium radiation enabled Fig. 10 to be composed for stagnation point conditions. The solid circles in Fig. 10 represent points obtained with shock-tube data and prediction techniques equivalent to that of the 1880 computer program for the spectral range $>0.2\ \mu$ and essentially optically thin conditions. The lower limit of $0.2\ \mu$ excludes the potential uncertainty caused by the fourth positive transition of the CO molecule. The open circles in Fig. 10 represent points determined from the 1880 computer run predictions adapted for comparison with somewhat more rigorous air calculation, both of which consider absorption and shock layer radiative cooling. The dip in the curve at about 39,000 ft/s is not completely understood, and for this reason the extended uncertainty curve (shown by the dashed line) is assumed. For the present analysis, however, a constant uncertainty factor of 1.4 is used for all cases (based on 0.85 V_E at V_E = 44,000 ft/s).

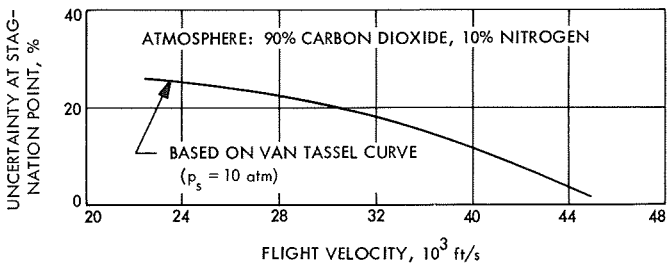

Fig. 8. Estimate of uncertainty in convective heat transfer calculations at stagnation point

IV. Analysis Constraints

The confidence in results of a heat-shield analysis is mainly dependent on two factors: (1) the adequacy of the computer program used in heat-shield performance calculations, and (2) knowledge of the required material properties. Both factors will be discussed at some length so that their significance in the analytical procedures employed in this report can be assessed.

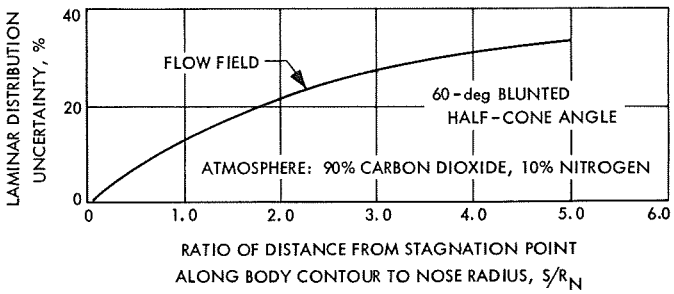

Fig. 9. Estimate of uncertainty in distribution of laminar convective heat transfer

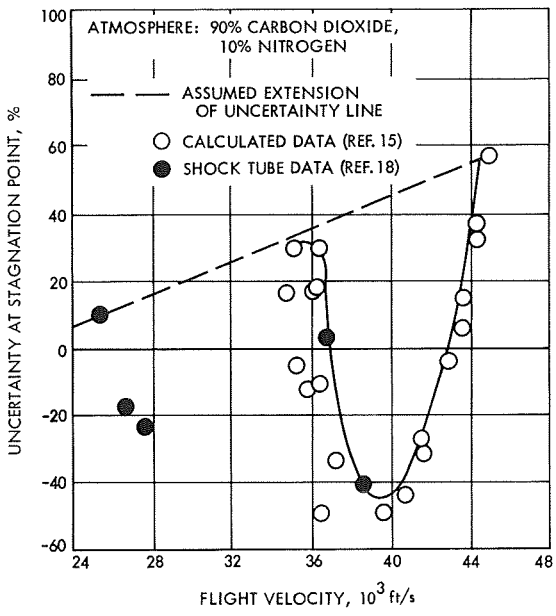

Fig. 10. Estimates of uncertainties in radiative heat transfer calculations

A. Review of Available Computer Programs Within NASA

In recent years a number of computer programs, available within NASA and dealing with the thermal response of the heat-shield material, have been acquired by JPL. These programs are:

Program Title	Source	Reference
CHAP I	Langley Research Center (LaRC)	19
CHAP II	LaRC	20
Stab 2	Manned Spacecraft Center (MSC)	21
1600	Avco Corp.	22
CMA	Aerotherm Corp.	23 and 24
REKAP	General Electric Co.	25

With the exception of REKAP, all these programs have been successfully operated to date at Jet Propulsion Laboratory. A study of characteristics of these programs revealed substantial differences when applied to the same problem.

In evaluating the computer program operation, it was necessary to start with the simplest environment (i.e., conduction only) and then gradually increase the severity of the environment in steps to observe the deviation between programs as the differences in handling the various functional operations or in mathematically representing the various thermal accommodation phenomena became effective. The total process is too lengthy to discuss here; however, as an example, Fig. 11 represents the cold wall convective heating for low-entry velocity into a Mars atmosphere (i.e., a low heating-rate condition). When this heat flux is used as an input to selected computer programs, the results obtained for the same material are those shown in Fig. 12. Variations shown are well-explained by different mathematical models and assumptions used in each program. Nevertheless, a need for allowing some uncertainties in computational techniques is thus apparent.

The Avco 1600 program was selected for the analysis in this study because, with exception of gaseous combustion, it represents with reasonable accuracy the physicochemical process of ablation. The versions of the CHAP I and CHAP II programs available at JPL do not provide for the material decomposition in depth and for

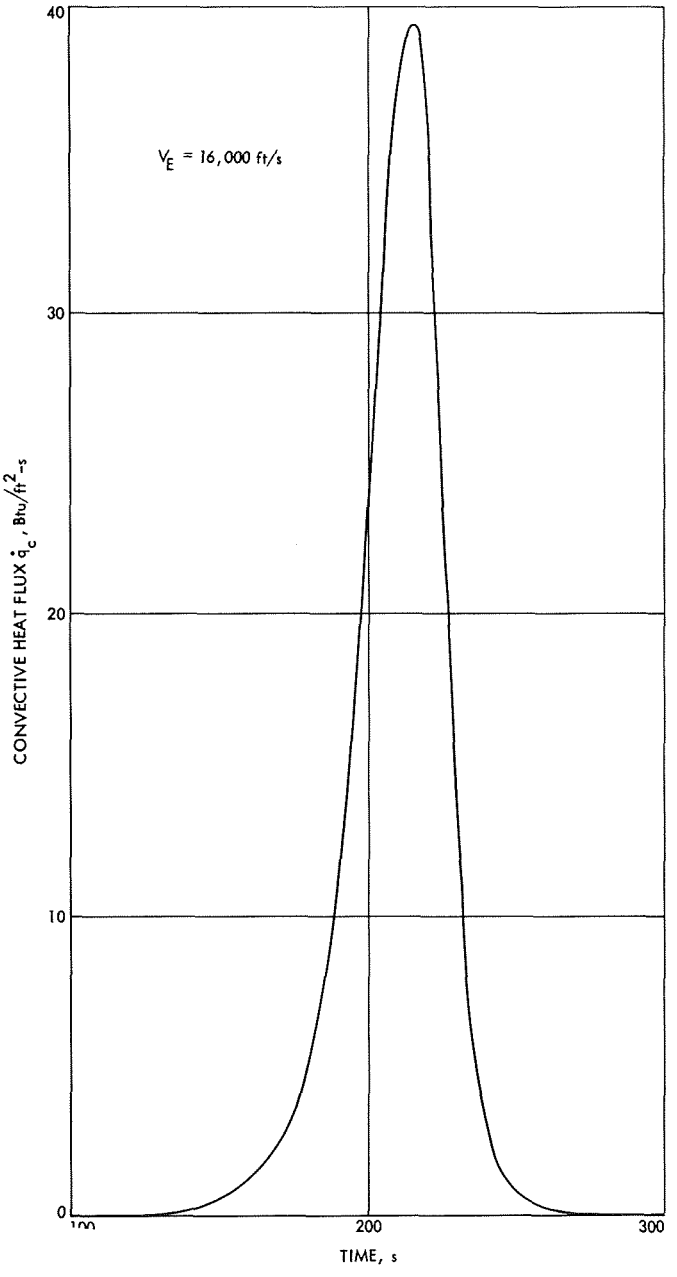

Fig. 11. Rate of convective heat transfer for Mars orbital entry

the surface char sublimation. In MSC Stab 2 decomposition in depth is not clearly defined and, as in Langley programs, no provision is made for char sublimation.

It appears that Langley and MSC programs were initially intended for the Apollo mission heat-shield performance calculations for which the somewhat idealized physicochemical model is used, but these programs can be modified so that they adequately represent anticipated

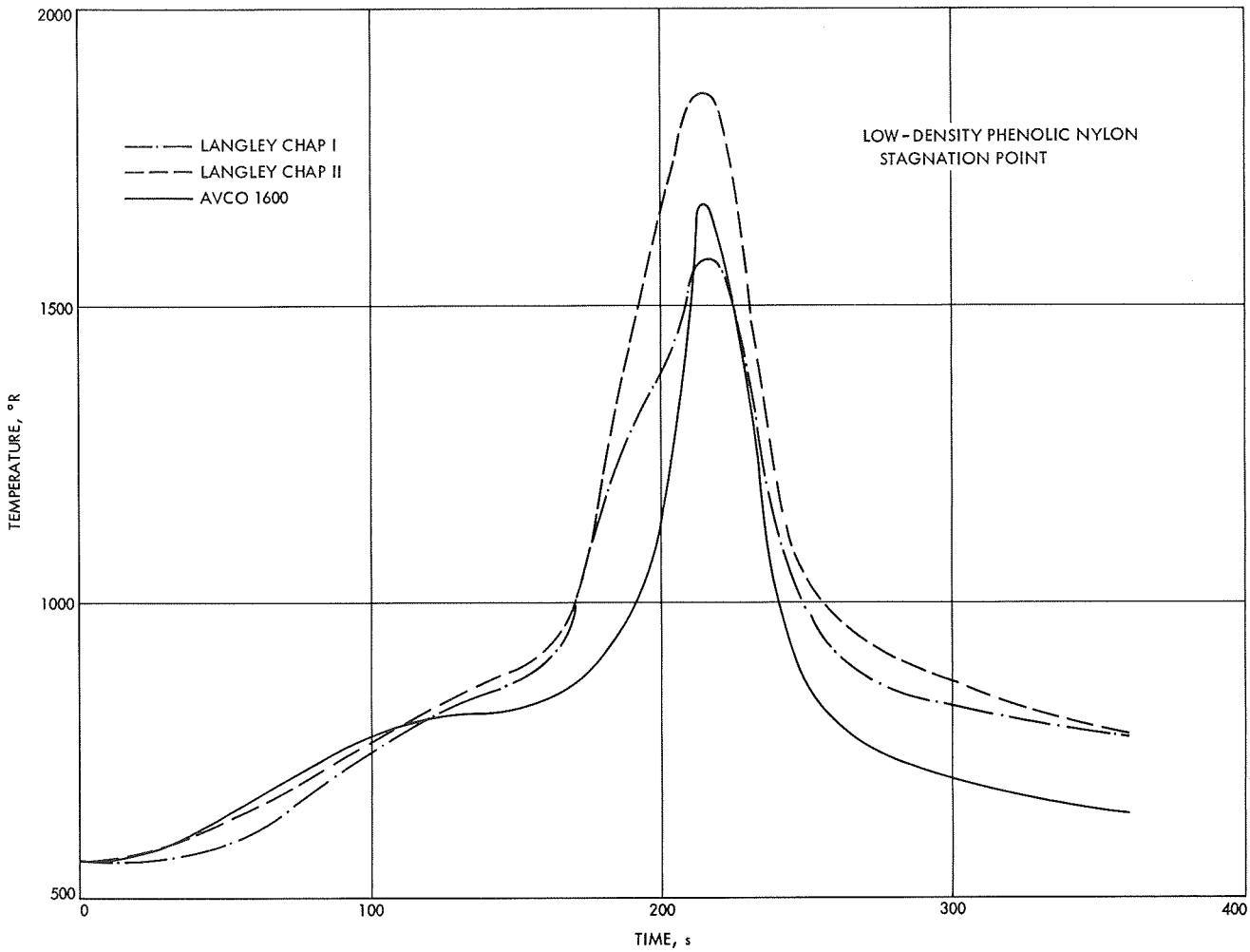

Fig. 12. Surface temperature as calculated by different computer programs

Venus entry environment. However, the object of this discussion is only to indicate computational uncertainties that might arise in selecting one program over the other, and to provide appropriate safeguards to cover such a contingency. Finally, the Aerotherm program requires an accurate knowledge of material chemistry to handle gaseous combustion. Computer runs were made comparing the Aerotherm program to the Avco 1600 program. Both programs gave comparable results (Fig. 13). Since the Avco program is considerably less expensive to operate, use of the Aerotherm program was discontinued for this study.

B. Review of Available Materials

For more than a decade, data on heat-shield materials were accumulated as a result of intensive research primarily directed toward military applications such as missile reentry cones. Subsequently, however, research embraced the heat-shield requirements for various NASA space programs.

A large number of materials were screened or developed to provide a suitable family of ablators applicable to a variety of planetary entry vehicles. Among the materials, the charring type offers the most economical protection against atmospheric entry heating.

With few exceptions, charring materials, applicable to entry heat shields, are plastic composites consisting of resin and binder, so their makeup is rather complex and in general lacks homogeneity. It is this latter characteristic, coupled perhaps with the tendency to decompose in a somewhat unpredictable manner, which makes it difficult to obtain reproducible material properties. In some cases there is even a lack of established standard procedures for measuring the property involved.

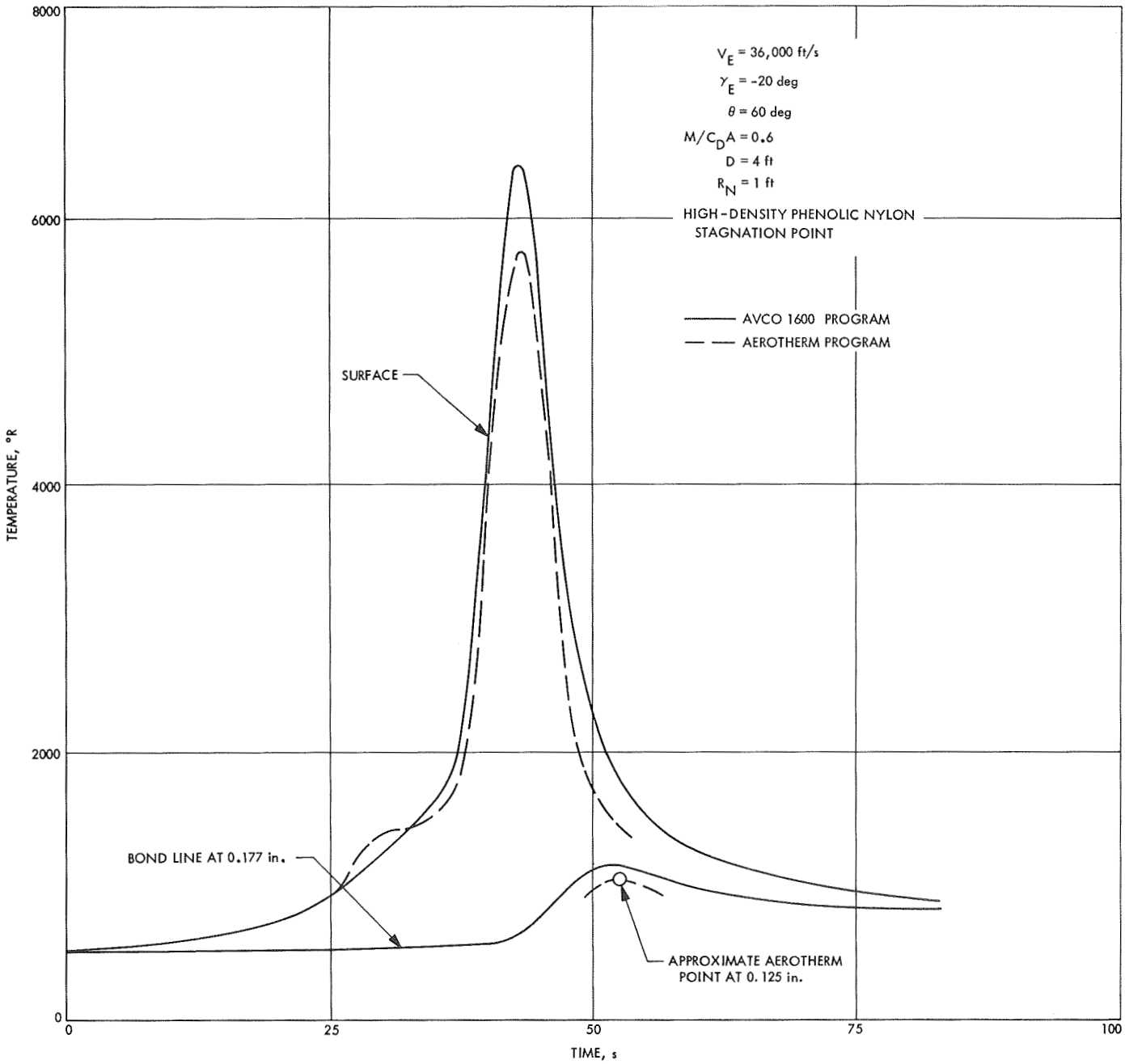

Fig. 13. Heat-shield temperatures for a Venus entry case

Figure 14 represents data on thermal conductivity and specific heat of a virgin carbon phenolic. These data were compiled at JPL from various sources with material descriptions essentially identical, and it is clear that the spread is very substantial. The same can be said about other typical materials such as phenolic nylons, silicone elastomers, etc.

The foresaid properties are not the only ones required for heat-shield analysis. In addition, the following properties are also needed to complete the analysis: thermal conductivity and specific heat of char; surface emittance of virgin material and char; heat of decomposition, specific heat of decomposition gases; laminar and turbulent blowing factors; decomposition rate constants of virgin material and char; sublimation constants of char; internal radiative heat absorption coefficient in char; and mechanical shear erosion information.

Although the list of materials that can be used for a Venus entry heat shield is quite substantial, the actual choice must be limited to those materials for which a complete set of data can be assembled. At the present time, these materials are low- and high-density phenolic nylons, silicone elastomers, Avcoat 5026-39/HC-G[3] and carbon phenolics.

C. Data Selection for Typical Materials

It is difficult to choose a set of data for each candidate material because of the lack of agreement in measurements as reported by various investigators. Some of the data are presented as a function of temperature and, when compiled, appear similar to that shown in Fig. 14. Most of the other data are given as constants, which are derived from optical, transpiration, thermogravimetric, and calorimetric measurements.

In view of the wide range of entry velocities and entry angles studied in this report, the typical representatives of all five materials mentioned above are considered. Table 2 lists the data used in the present analysis. These data were taken from a large variety of sources after due consideration of the most probable value from the available measurements for each property. In some cases where no rationale of judgment was available, a conservative value was chosen and the uncertainty band was adjusted accordingly to allow for the bias. In addition, the following sublimation constants for carbonaceous char are used for all of the typical materials selected:

$$\beta' = 1.82 \times 10^7 \text{ ft/s } {}^\circ\text{R}^{\beta''}$$

$$\beta'' = 0.28$$

$$\beta''' = 1.61 \times 10^5 {}^\circ\text{R}$$

These constants are required for the calculation of char recession rates caused by sublimation. The recession rate equation, as postulated in Vol. 1 of Ref. 22 is

$$\dot{s}_s = \bar{B}\,\beta'\,T_s^{\beta''} \exp\left(-\frac{\beta'''}{T_s}\right) \tag{1}$$

The correction factor $\bar{B}$ for recondensation is a function of temperature and pressure, and is subject to large uncertainties at very high heat loads.

The thermal conductivity and specific heat data given in Table 2 are for the initial and charred states of the material. For an intermediate state (decomposition), it is assumed that actual values are also dependent on local material density. The accepted expressions used in computation are given by

$$k = k_v + (k_c - k_v)\, r_k \tag{2}$$

and

$$c_p = c_{p_v} + (c_{p_c} - c_{p_v})\, r_c \tag{3}$$

where r_k and r_c are functions of local density with the following limits:

$$r_k = r_c = 0 \qquad \text{for } \rho = \rho_v$$

$$r_k = r_c = 1.0 \qquad \text{for } \rho = \rho_c$$

Normally, a linear relationship is assumed between these limits. However, Ref. 5 gives the following nonlinear values for X6300 carbon phenolic: These values are listed in Table 3.

[3]Epoxy-novalac resin with phenolic microballoons and silica fiber reinforcement in a fiberglass reinforced-phenolic honeycomb matrix.

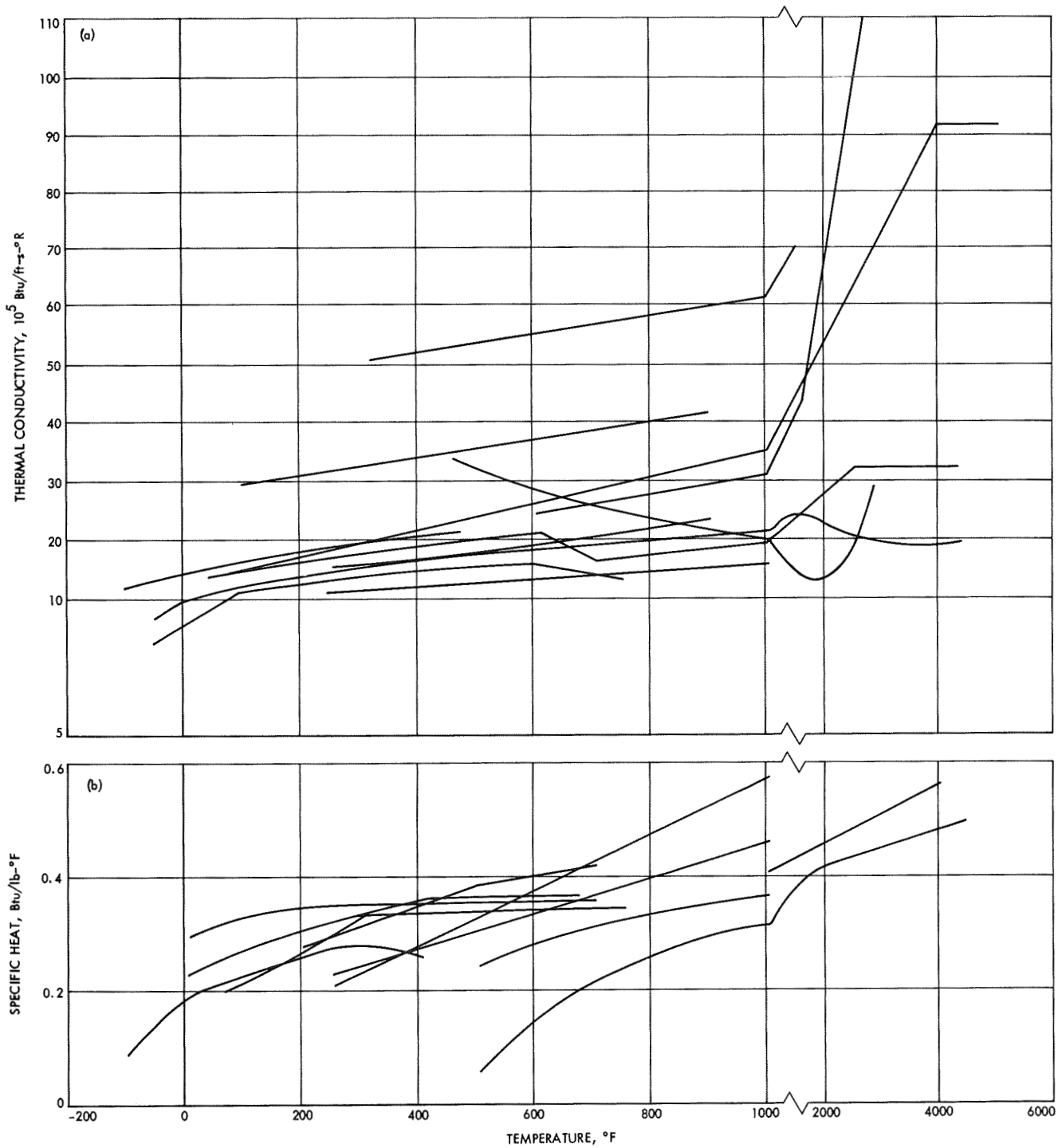

Fig. 14. Variation in available data for carbon phenolic with 35% resin content: (a) thermal conductivity; (b) specific heat

Table 2. Thermo-ablation properties of typical materials

Property name (units)	Materials				
	Low-density phenolic nylon	High-density phenolic nylon	Avcoat 5026-39/HC-G	Carbon phenolic (X6300)	Foamed silicone elastomer
Composition by weight	50–50	50–50	—	—	—
Density of virgin material, lb/ft^3	35.0	75.0	33.0	90.0	35.0
Char density, lb/ft^3	13.1	22.5	16.5	60.0	14.4
Carbon weight fraction:					
Virgin material	0.25	0.25	0.242	0.40	0.35
Char	0.67	0.84	0.49	0.71	0.71
Thermal conductivity of virgin material,[a] Btu/ft-h-°R	260°R 0.0575 460°R 0.0505 780°R 0.0515 900°R 0.061 1,360°R 0.061	500°R 0.155 870°R 0.155 1,280°R 0.097 1,360°R 0.061	0.140	500°R 0.33	540°R 0.081 860°R 0.122 1,335°R 0.158 1,710°R 0.187
Char thermal conductivity,[a] Btu/ft-h-°R	400°R 0.360 1,000°R 0.505 3,300°R 1.260 4,000°R 1.370	500°R 0.500 2,400°R 0.835 3,700°R 1.140 4,700°R 2.580	460°R 0.140 1,660°R 0.140 1,860°R 0.220 2,260°R 0.355 2,460°R 0.425 2,860°R 0.540 3,060°R 0.595 3,460°R 0.700	500°R 0.375 2,960°R 1.130	540°R 0.079 1,335°R 0.533 1,710°R 0.610 2,210°R 0.720 6,000°R 0.720
Specific heat of virgin material,[a] Btu/lb-°R	260°R 0.20 460°R 0.29 860°R 0.57 1,300°R 0.58	200°R 0.045 400°R 0.390 600°R 0.445 800°R 0.500 1,260°R 0.500	460°R 0.385 660°R 0.440 960°R 0.520 1,160°R 0.575 1,360°R 0.655	0.250	540°R 0.30 800°R 0.39 1,000°R 0.43 2,000°R 0.44
Char specific heat,[a] Btu/lb-°R	400°R 0.52 5,000°R 0.52	500°R 0.200 2,000°R 0.630 5,000°R 0.670	1,360°R 0.655	660°R 0.260 1,460°R 0.538	540°R 0.20 1,400°R 0.30 2,000°R 0.44 6,000°R 0.60
Specific heat of decomposition gas,[a] Btu/lb-°R	400°R 0.60 2,000°R 0.60 2,250°R 0.50 2,750°R 0.30 6,000°R 0.30	400°R 0.60 2,000°R 0.60 2,200°R 0.50 2,750°R 0.30 6,000°R 0.30	540°R 0.550 1,000°R 0.660 2,000°R 0.740 3,000°R 0.790 4,000°R 0.830 8,000°R 0.960	0.40	0.384
Surface emittance	0.8	0.8	0.667	0.8	0.85
Surface absorptance	1.0	1.0	1.0	1.0	1.0
Laminar blowing factor	0.6	0.6	0.7	0.76	0.6
Turbulent blowing factor	0.4	0.4	0.37	0.4	0.4
Combustion enthalpy, Btu/lb	12,000	12,000	11,850	16,100	12,000
Heat of vaporization, Btu/lb	10,000	10,000	11,400	11,400	10,000
Heat of decomposition, Btu/lb	1,000	1,000	500	600	450
Decomposition reaction constants:					
n	1.0	1.0	2.5	1.0	2.0
A, s^{-1}	7.8×10^{12}	7.8×10^{12}	3.44×10^{4}	1,500	3.0×10^{4}
B, °R	43,200	43,200	21,800	10,000	24,000

[a]Wherever data are available, properties are given as a function of temperature.

Table 2 (contd)

Property name (units)	Materials				
	Low-density phenolic nylon	High-density phenolic nylon	Avcoat 5026-39/HC-G	Carbon phenolic (X6300)	Foamed silicone elastomer
Reaction rate combustion constants:					
n'	0.5	0.5	0.5	0.5	0.5
A', $lb/ft^2\text{-}s\text{-}atm^{0.5}$	6.73×10^8	1.74×10^5	10.325	7.00×10^8	6.73×10^8
B', °R	39,877	36,200	11,260	40,000	39,877

Table 3. Density functions for X6300 carbon phenolic

Local material density ρ, lb/ft^3	Thermal conductivity function, r_k	Local material density ρ, lb/ft^3	Specific heat density function, r_c
60.0	1.0	60.0	1.0
68.0	1.0	72.0	1.0
76.5	2.0	90.0	0.0
90.0	0.0	—	—

D. Uncertainties in Material Properties

The number of material properties involved is rather substantial, and inclusion of their various effects, based on experimental spread of data, would result in a prohibitive matrix of cases to be investigated, especially when coupled to the extensive entry-trajectory matrix derived earlier.

The approach taken here is to first evaluate the selected typical materials, with regard to their applicability for various Venus entry environments from points of thermal and weight considerations, then to apply uncertainty analysis to the materials finally chosen for heat-shield applications.

A material property that has the most significant effect on sizing a heat shield is the thermal conductivity. Yet the available experimental data compiled from various sources indicate that this property, for some materials, has an uncertainty factor of more than two. Next in importance is the specific heat; however, the spread in experimental data is not as wide as that for thermal conductivity. All the other properties affect heat-shield thickness in varying degrees and their influence must be taken into account.

Uncertainties also exist in the material response to surface sublimation at very high temperatures and in the thermophysical balance of the process when coupled with internal decomposition. This subject will be dealt with to some extent in the next subsection.

For reasons just discussed, the uncertainty analysis cannot be generalized without severe weight penalties that may ensue, but it must apply to each individual material subjected to the actual range of entry environments in a given planetary atmosphere.

E. Sublimation Effects

Since sublimation has a particularly influential effect on heat-shield requirements for several Venus missions, the individual peculiarities of handling this parameter are discussed separately here. The sublimation of carbon and graphites has been studied extensively in recent years (Refs. 26–28). Yet, at the present time there appears to be no reliable formulation describing the process. The main difficulty seems to be in the adequate presentation of carbon-species recondensation, which requires knowledge of the partial pressures for the carbon-vapor species in the flow field. The accommodation coefficient (probability of attachment to the surface by collision) is also uncertain.

In the Avco 1600 program, the correction coefficient $\bar{B}$ for recondensation (Eq. 1) appears to give satisfactory results for moderate heating levels. However, when high radiative heat flux is applied and the convective heating is completely or nearly blocked, erroneous results are obtained and cause an abort of the computer run. This problem is normally corrected by assuming sublimation into vacuum ($\bar{B} = 1$). When this assumption is made, the results appear to be conservative and provide some safety factor.

Another aspect of importance is the interaction between surface sublimation and internal decomposition. Both phenomena are time-dependent but are governed

by different mechanisms. At very high heating rates, continuing to rise after the onset of sublimation, surface recession becomes very high and char may be consumed at a faster rate than internal decomposition can produce it. This is quite probable in the materials of low thermal conductivity wherein the temperature profiles are very steep at the points close to the surface. The resulting effect of this phenomenon would be the direct evaporation of virgin material.

The above phenomenon has been encountered during the course of the present analysis at the very high radiative heating rates representative of 44,000 ft/s. A number of aborted runs were attributed to the fact that, as the char was consumed more rapidly than it was produced, the surface began to recede into yet uncharred material. Consequently, the density of the material near the surface was increasing from its charred value to the value of the virgin material. Just before virgin density (80–90%) was reached, the material nodes at the surface became so exceedingly thin that the numerical technique of this particular computer program, for all practical purposes, was incapable of solution. This phenomena is also common to most of the other programs.

The problem just described has been overcome for this study by hypothesizing that the said phenomenon, revealed by analysis, might be real. At the time the material density was reverting to its virgin value, the decomposition mechanism in the program was stopped for a fraction of a second, after which time the decomposition was reinstated. This method has allowed the material density at the surface to assume its virgin value for a very short time, and the heat flux could then reshape the temperature profiles in-depth, so that the stable ablation process, including decomposition, could be resumed. By this device, computer run aborts were eliminated and all runs were successfully completed.

Since the material density was allowed to assume its virgin value, the result was a somewhat deeper heat penetration, and the effect of such an operation on heat-shield performance is obviously conservative; this fact, together with the assumed conservative sublimation process, should insure adequate safety.

Sublimation has yet another effect on heat-shield performance when radiative heat flux is very high and convective heating is practically blocked by the ablation gaseous products. Figure 15a is a plot of the radiation heating rate for an entry at 44,000 ft/s, and Fig. 15b indicates corresponding surface weight loss. It is seen

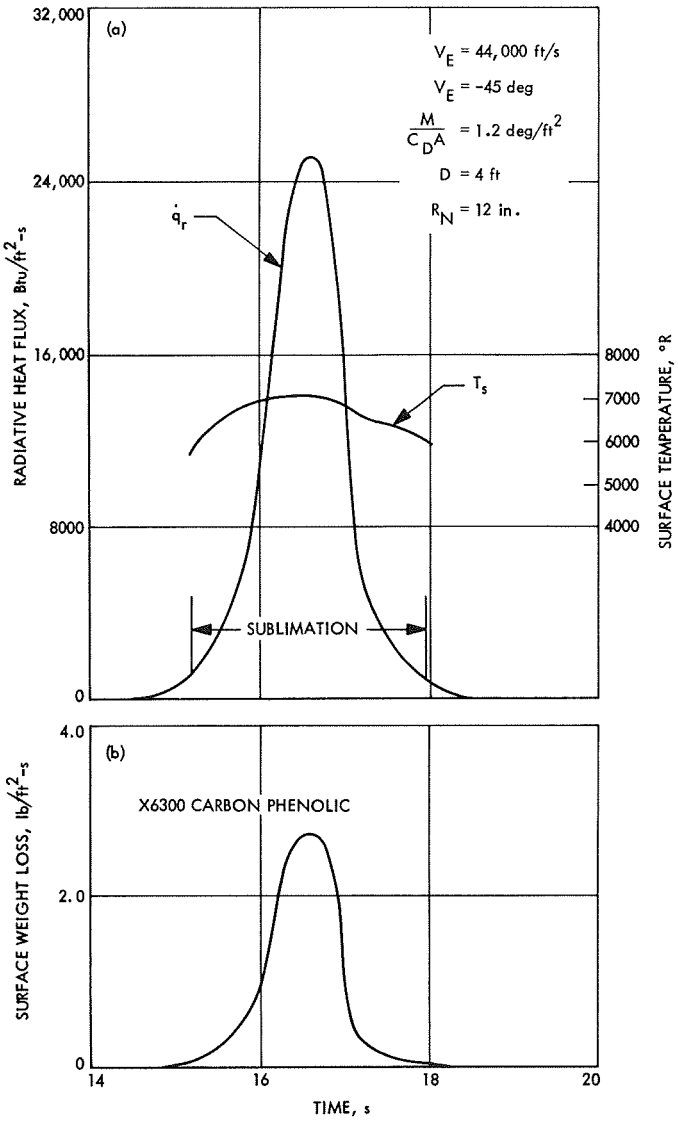

Fig. 15. Radiative heating and surface weight loss: (a) radiative heat flux; (b) surface weight loss

that weight loss is almost entirely due to sublimation. Also included in Fig. 15 is the surface temperature that indicates a change of approximately 15% during the radiative heat pulse. Thus, while the radiative flux is increasing very rapidly, the heat rejection by reradiation is relatively constant and the absorption of heat is caused by only the endothermic process of sublimation and results in high char consumption.

To further illustrate the influence of high char consumption on heat-shield performance, Table 4 presents an example of dimensional relationship at the stagnation point for two entry velocities and different material in

Table 4. Examples of surface recession during sublimation

Entry velocity V_E, ft/s	Material	Surface recession s, in.	Stagnation point heat-shield thickness δ, in.
36,000	Avcoat 5026-39/HC-G	0.181	0.264
44,000	X6300 carbon phenolic	0.415	0.535

each case. These data are for entry angle $\gamma_E = -45$ deg and ballistic coefficient of 1.2. The heat-shield thickness δ_0 is based on bond-line requirements (see next subsection). Clearly, the difference between the initial heat-shield thickness and the surface loss s appears to be adequate; however, for very low thermal conductivity materials, some 10% of calculated nominal heat-shield thickness (originally calculated by the computer programs) should be added after applying an overall uncertainty factor.

F. Structure Effects

Normally, a heat shield is attached to the vehicle structure by a bonding method that imposes a maximum temperature limit at the bond line to preserve an adequate strength of the bond. For the present day bonding compounds, this temperature limit is approximately 600°F (1060°R). Because of this, the heat-shield thickness is calculated so that at no point on the vehicle will its backside temperature exceed the above limit under actual entry conditions (to approximately Mach 0.5).

A vehicle structure (including bond thickness), whatever its design, will have a heat storage capacity and will be able to conduct as well as exchange heat with the interior of the vehicle. Therefore, the design of the structure will have an effect upon heat-shield material performance.

In making allowance for structure effects in this type of general treatment, some approximation is inevitable, since in reality a considerable number of structure designs could be conceived. For the purpose of actual heat-shield thickness determination, it was assumed that heat-shield material consists of a slab whose initial thickness is somewhat in excess of bond-line temperature limit requirements, and whose backside wall radiates to a quiescent environment kept at a temperature of 80°F (540°R). The initial slab temperature distribution was constant and equal to 80°F. It is presumed that this excess in slab thickness, judiciously allowed under the described conditions, should adequately compensate for the structure effects.

V. Heat-Shield Requirements

Heat-shield materials are characterized by their ability to resist the in-depth penetration of heat when exposed to a severe thermal environment. In charring materials, this ability is derived from the endothermic processes such as internal decomposition and surface sublimation, surface reradiation, and low thermal conductivity. For Venus entries at high angles and velocities, the sublimation becomes an important factor in the calculation of heat-shield performance.

After candidate heat-shield materials have been selected, and the factors of safety to cover the known uncertainties have been established, design data can be computed and presented in graphical or tabular form.

A. Comparison of Typical Material Alternatives

The wide range of entry conditions typical of Venus entry imply that one heat-shield material is not likely to be optimum for all missions. With material properties generally unavailable in a complete form, the designation of an optimum material for any individual mission is by no means an easy task. On the other hand, the five materials discussed earlier with complete or reasonably complete data represent an adequate spectra of densities and material compositions, and can be used on a first-cut basis as standards of comparative performance for later material development.

A comparison of the performance of the five "standard" materials is provided in Table 5. Only the lower-entry velocity conditions are compared. These data were obtained for ballistic coefficients of 0.6 slug/ft^2, and were based on an assumed maximum heat-shield–structure bond-line temperature. The data present a relative assessment only because safety factors and other allocations were not included. For these conditions, the three low-density materials provide approximately comparable performance. In the higher energy entries shown in Table 5, the elastomeric and the low-density phenolic nylon tend to be shear sensitive and the performance shown could be optimistic. The Avcoat 5026-39/HC-G, on the other hand, is protected somewhat from shear by a honeycomb support matrix and is known to perform adequately under these flight conditions. All further calculations for

Table 5. Comparison of performance of typical heat-shield materials[a]

Material	V_E, ft/s	γ_E, deg	ρV, lb/ft^3	δ_0, in.[b]	W/A_0, lb/ft^2
Avcoat 5026-39/HC-G	36,000	−45	33	0.181	0.490
High-density phenolic nylon			75	0.110	0.700
Low-density phenolic nylon			35	0.188	0.548
X6300 carbon phenolic			90	0.177	1.330
Foamed silicone elastomer		−45	35	0.195	0.570
Avcoat 5026-39/HC-G		−20	33	0.231	0.632
High-density phenolic nylon			75	0.159	0.990
Low-density phenolic nylon		−20	35	0.235	0.684
Avcoat 5026-39/HC-G	32,000	−45	33	0.161	0.442
High-density phenolic nylon			75	0.092	0.574
Low-density phenolic nylon			35	0.159	0.465
X6300 carbon phenolic			90	0.162	1.22
Foamed silicone elastomer		−45	35	0.178	0.520
Avcoat 5026-39/HC-G		−20	33	0.223	0.612
High-density phenolic nylon			75	0.148	0.927
Low-density phenolic nylon		−20	35	0.200	0.580

[a] M/C_DA = 0.6 slug/ft^2.

[b] These data should be used only for relative assessment as they do not include appropriate safety factors and other allowances.

low-entry velocity trajectories are made with the Avcoat 5026-39/HC-G material.

For shears above 15 lb/ft^2 (based on a flow field without ablation), the honeycomb-reinforced Avcoat material displays an irregular char recession that is not included in this analysis. At a higher energy entry, high-shear resistant materials must be utilized. The carbon phenolic material is necessary at 44,000 ft/s although there may be some doubt regarding its shear sensitivity at the high pressures typical of these entry conditions.

There is a probability that high density phenolic nylon is better able to resist shears above 15 lb/ft^2 than is the Avcoat material, therefore its use might be extended to entries with higher ballistic coefficients. In this study, all higher velocity entry performances (above 36,000 ft/s) were calculated using only X6300 carbon phenolic.

B. Manufacturing Considerations

Before a designer specifies the dimensions for a specific heat shield, some consideration must be given to the manufacturing tolerances possible or inherent in the construction materials. The shapes investigated are all sphere-cones with heat-shield requirements calculated at only the center point, the tangent line between the sphere and the cone, and near the outer edge. All thicknesses are considered to be linearly extrapolated between calculation points.

Pure analysis does not take into account the mismatch between manufacturing capability and dimensional line drawings. In vehicles of the size considered here, the structural base for the heat shield tends to be slightly distorted, and the distortion grows with size.

In this study the manufacturing tolerances of the heat shield are assumed to be ± 0.02 in. This assumption tends to be somewhat optimistic but is considered to be a fair balance between real tolerances and severe weight penalties. To allow for this manufacturing contingency, 0.02 in. has been added to the calculated heat shield after all other uncertainties have been accounted for.

C. Safety Factor Criteria

For a heat-shield design to be safe, allowances must be made for all of the probable uncertainties. A summation of the uncertainties discussed in earlier sections is

provided in Table 6. These uncertainty factors are derived from the inspection of scatter in experimental data or from the difference in constants as reported in technical literature. The listed material-property uncertainty factors have been reasonably ascertained for Avcoat and X6300 carbon phenolic used in this analysis; for other materials, different factors may apply. Based on these assumed independent errors, a standard increment to the nominal value calculated by the computer program may be deduced.

The performance errors are derived from a consideration of the change in heat-shield requirement for a particular nominal trajectory if only that property were changed from the nominal data. Example variations for conductivity, specific heat, and emittance are provided in Figs. 16, 17, and 18. When the thermal conductivity was doubled, the heat-shield requirement changed by approximately 30%. The effect of other properties was less significant.

These performance errors may then be collected together according to the theory of error discussed in Ref. 29. With all of the deviations being essentially linear, the total maximum probable error becomes

$$\Delta\delta = (\Delta\delta_k^2 + \Delta\delta_{c_p}^2 + \cdots)^{1/2} \tag{4}$$

where $\Delta\,\delta_k$, $\Delta\,\delta_{c_p}$, etc. are individual uncertainties caused by thermal conductivity, specific heat, etc. The values of these uncertainties for Avcoat 5026-39/HC-G at an entry velocity of 36,000 ft/s are given in Table 6. The calculated statistical factors of safety for the nominal trajectories are shown in Fig. 19. Based on these results, a

Table 6. Uncertainties with respect to nominal values

Parameter	Uncertainty factor		Avcoat 5026-39/HC-G (V_E = 36,000 ft/s)	
	Low limit	High limit	Thickness uncertainty, in.	Thickness uncertainty factor
Material thermal conductivity	0.75	2.0	0.060	1.300
Material specific heat	0.75	1.5	0.020	1.100
Specific heat of decomposition gas	0.75	1.25	0.010	1.050
Surface emittance	0.75	1.25	0.013	1.065
Laminar blowing factor	0.75	1.15	0.016	1.080
Turbulent blowing factor	0.75	1.15	0.020	1.100
Heat of decomposition	0.50	2.0	0.005	1.025
Material decomposition rate	0.50	1.5	0.004	1.020
Reaction regime char recession rate	0.50	1.5	0.003	1.015
Internal absorption of radiation	0	300[a]	0.002	1.010
Mechanical erosion	0	90% of char extinction	0.020	1.100
Cold wall convective heating (laminar)	—	Fig. 9	0.015	1.075
Cold wall convective heating (turbulent)	—	1.2	0.014	1.075
Radiative heating	—	1.4	0.017	1.085
Wall enthalpy	—	1.1	0.004	1.020
Computer program technique	—	10% of thickness	0.020	1.100
Others (sublimation constants, etc.)	—	10% of thickness	0.020	1.100

[a]Assumed probable value for absorption coefficient.

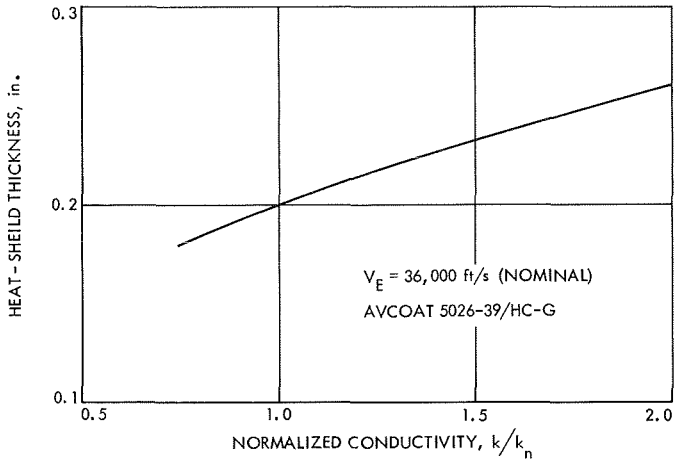

Fig. 16. Dependence of heat-shield thickness on material thermal conductivity

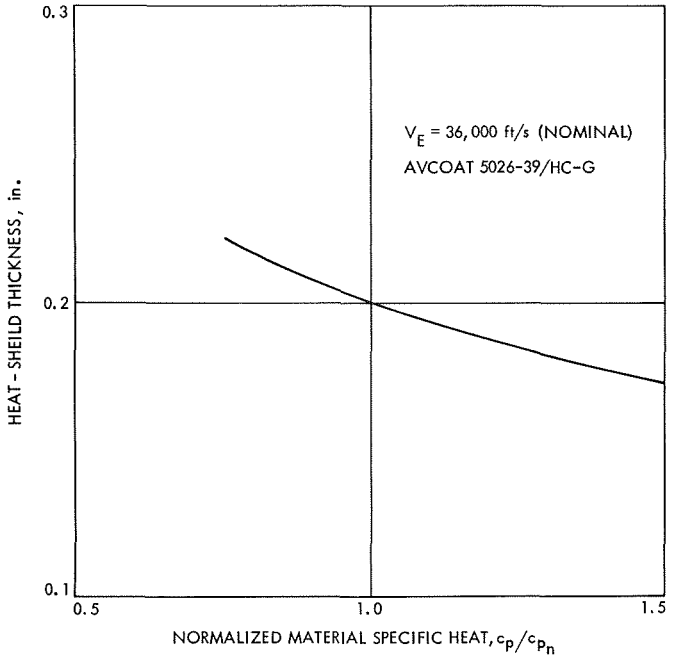

Fig. 17. Dependence of heat-shield thickness on material specific heat

constant factor of 1.5 was assumed for all cases[4]. In addition, the calculated heat-shield requirements with the factor of safety incorporated are increased by 0.02 in. to account for manufacturing uncertainties. Furthermore, 10% of the nominal value has been added around the outer shoulder because of uncertainty in shear analysis in this area.

[4]Safety factor f is calculated by $f = (\delta_n + \Delta\delta)/\delta_n$.

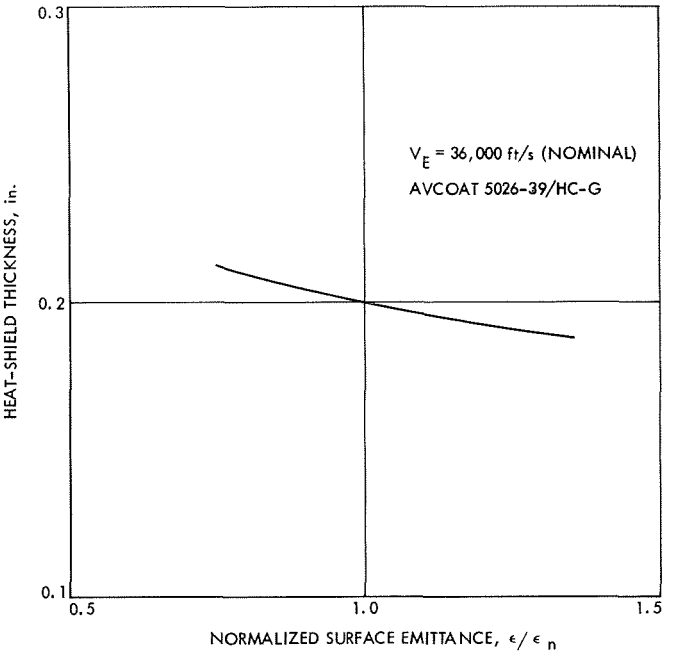

Fig. 18. Dependence of heat-shield thickness on surface emittance

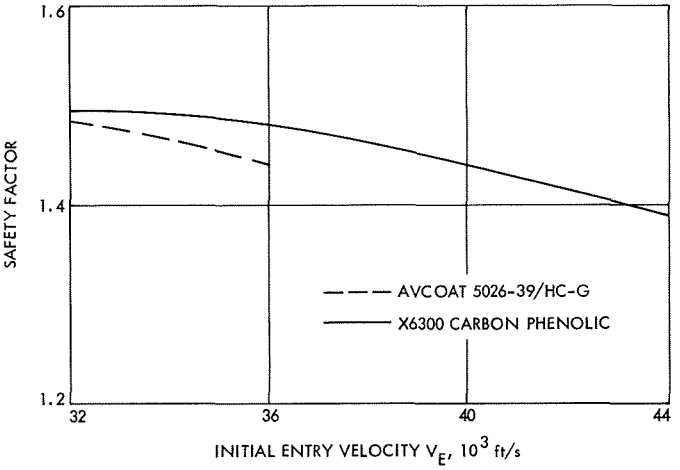

Fig. 19. Safety factors for nominal trajectories

D. Comparison for Trajectory Alternatives

The heat-shield requirements for each trajectory variation are given in Table 7. The three thicknesses δ represent the requirements at the stagnation point, at the junction of the sphere cone, and at the outer shoulder, respectively. The apparent similarity between the heat-shield requirements at all three points is caused by higher radiant heating rates, a generally normal transition to turbulence just after peak convective heating, and increased uncertainty allowances for various other factors. Figure 20 indicates the assumed heat-shield

Table 7. Heat-shield dimensional and weight data for trajectory alternatives

Trajectory data						Avcoat 5026-39/HC-G					X6300 carbon phenolic				
Computer run	V_E, ft/s	M/C_DA, slug/ft^2	γ_E, deg	D, ft	R_N, in.	δ_0, in.	δ_j, in.	δ_{sh}, in.	W/A_s, lb/ft^2	W/W_t	δ_0, in.	δ_j, in.	δ_{sh}, in.	W/A_s, lb/ft^2	W/W_t
1	32,000	0.3	−20	4	12	0.335	0.326	0.330	0.88	0.069	0.316	0.306	0.309	2.25	0.176
2			−45			0.262	0.253	0.268	0.71	0.056	0.248	0.238	0.252	1.82	0.143
3			−90			0.230	0.219	0.242	0.63	0.050	0.216	0.205	0.227	1.62	0.127
4		0.6	−20			0.380	0.367	0.386	1.01	0.040	0.357	0.344	0.361	2.59	0.101
5			−45			0.280	0.278	0.290	0.77	0.030	0.263	0.262	0.272	1.97	0.077
6			−90			0.253	0.246	0.282	0.73	0.029	0.238	0.232	0.264	1.87	0.073
7		1.2	−20			0.428	0.394	0.465	1.18	0.023	0.402	0.371	0.435	3.01	0.059
8			−45			0.341	0.320	0.446	1.08	0.021	0.320	0.301	0.418	2.78	0.054
9			−90	4	12	0.321	0.307	0.324	0.86	0.017	0.300	0.284	0.351	2.41	0.047
15	36,000	0.3	−20	4	12	0.351	0.342	0.358	0.94	0.074	0.322	0.314	0.326	2.36	0.185
16			−45			0.268	0.264	0.293	0.76	0.060	0.246	0.243	0.267	1.91	0.149
17			−90			0.236	0.225	0.253	0.66	0.052	0.217	0.208	0.230	1.64	0.129
18		0.6	−20			0.391	0.377	0.409	1.06	0.042	0.357	0.346	0.372	2.65	0.104
19			−45			0.312	0.296	0.321	0.84	0.033	0.286	0.270	0.292	2.09	0.082
20			−90			0.294	0.281	0.327	0.84	0.033	0.270	0.259	0.280	2.01	0.079
21		1.2	−20			0.504	0.426	0.561	1.37	0.027	0.461	0.389	0.510	3.42	0.067
22			−45			0.445	0.422	0.524	1.30	0.026	0.406	0.386	0.473	3.23	0.063
23			−90	4	12	0.428	0.401	0.465	1.18	0.023	0.391	0.367	0.422	2.94	0.058
29	44,000	0.3	−20	4	12	—	—	—	—	—	0.330	0.301	0.299	2.20	0.172
30			−45								0.271	0.232	0.252	1.81	0.142
31			−90								0.268	0.212	0.243	1.73	0.136
32		0.6	−20								0.392	0.340	0.375	2.66	0.104
33			−45								0.443	0.271	0.340	2.36	0.093
34			−90								0.476	0.260	0.328	2.29	0.090
35		1.2	−20								0.728	0.405	0.514	3.52	0.069
36			−45								0.826	0.413	0.546	3.71	0.073
37			−90	4	12						0.693	0.414	0.559	3.75	0.073

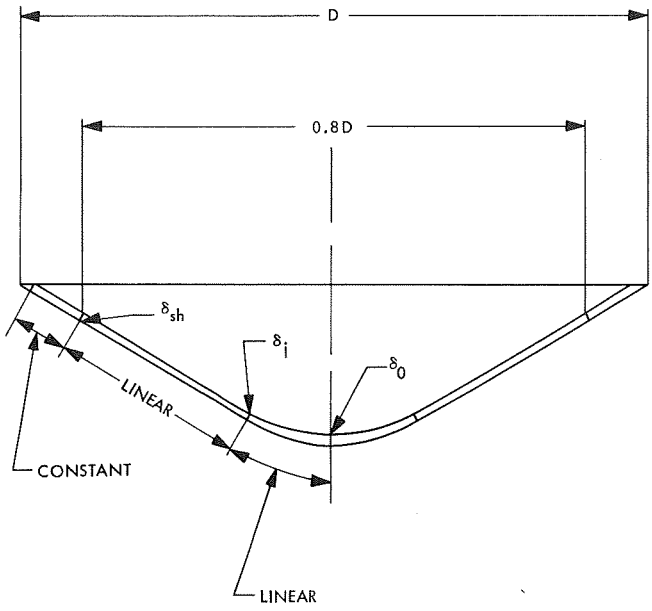

Fig. 20. Heat-shield geometry

geometry. The unit weight (W/A_s) column represents the heat-shield weight divided by the forward surface area of the blunted cone. The last column for each material represents the fraction of the total entry weight required as heat shield. All values include the appropriate safety factors discussed earlier.

To facilitate interpolation for entry cases not specifically included in Table 7, a series of charts has been plotted delineating the results as a function of entry velocity, entry angle, and ballistic coefficient. Figures 21–24 provide unit-weight plots to aid in relating entry-vehicle size to heat-shield weight requirements. Figures 25–28 provide weight-fraction plots to establish perspective for rapid design of different entry weights. By proper cross-reading or cross-plotting, heat-shield requirements for any combination of entry conditions can be obtained within the range investigated. Judicious use of these charts can substantially simplify the effort in the initial project stage. If design cases vary substantially from the nominal cases, single-check runs can be made at critical stages in the mission design to verify accuracy. Care should be taken to incorporate the same or, if better data are available, a better factor of safety than that delineated in the previous section.

From the charts, several observations may be made. Entry angle affects time of exposure and, in most cases,

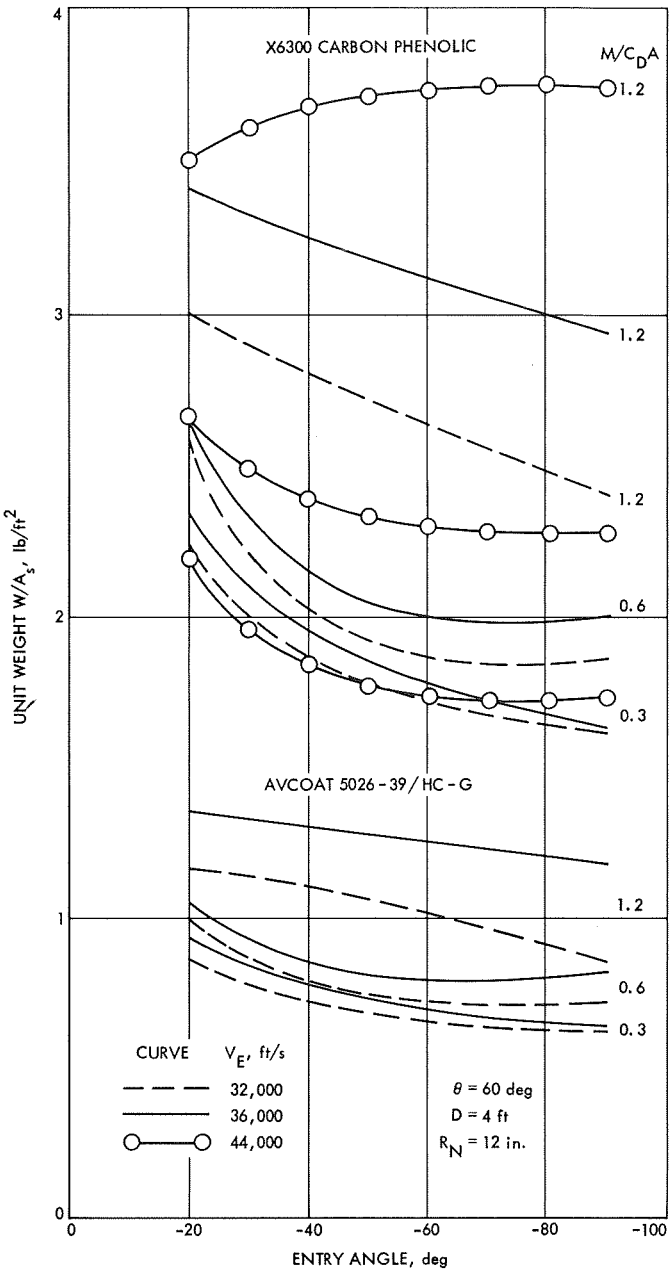

Fig. 21. Effect of entry angle on heat-shield unit weight

increases the weight fraction as the peak energy load decreases, but the integrated heating increases. Unit weight increases with an increasing ballistic coefficient as the entry environment becomes more severe. On the other hand, a higher ballistic coefficient for a constant diameter results in increased total weight available with attendant decrease in the heat-shield weight fraction. Care must be taken in the use of these charts to transfer

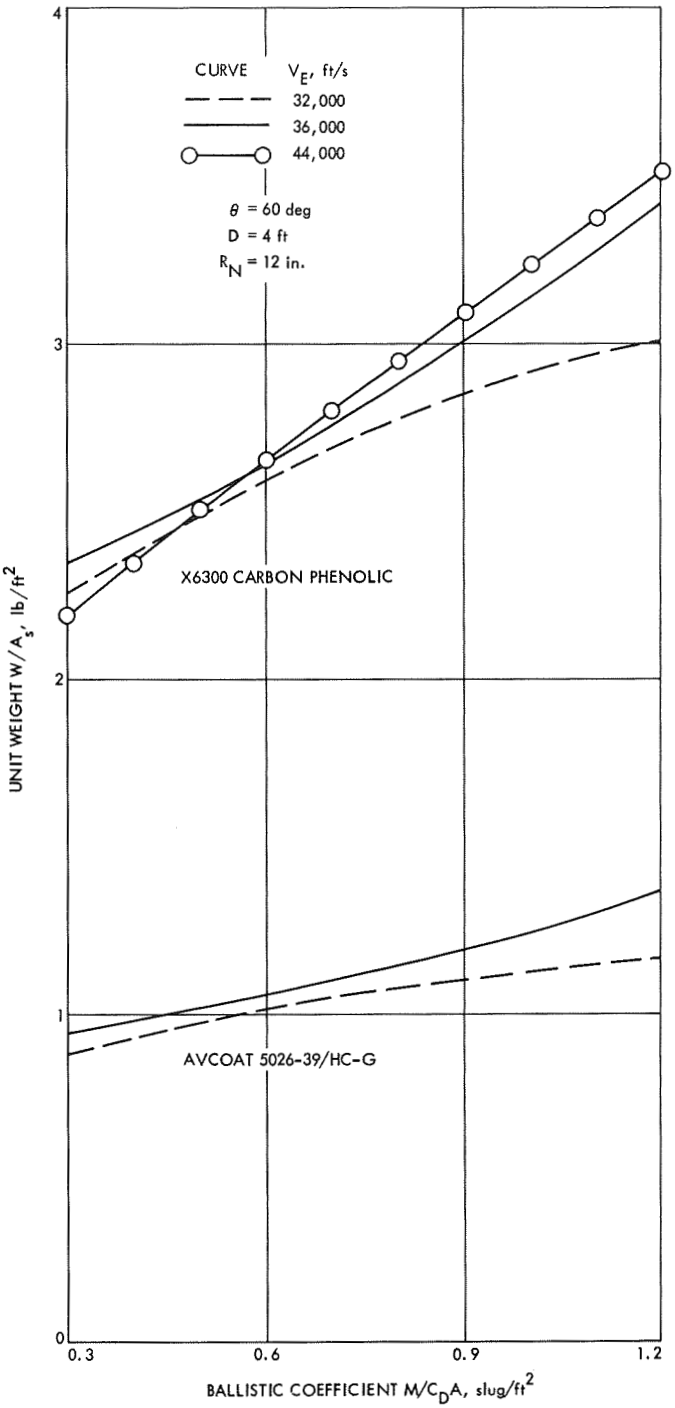

Fig. 22. Effect of ballistic coefficient on heat-shield unit weight, $\gamma_E = -20$ deg

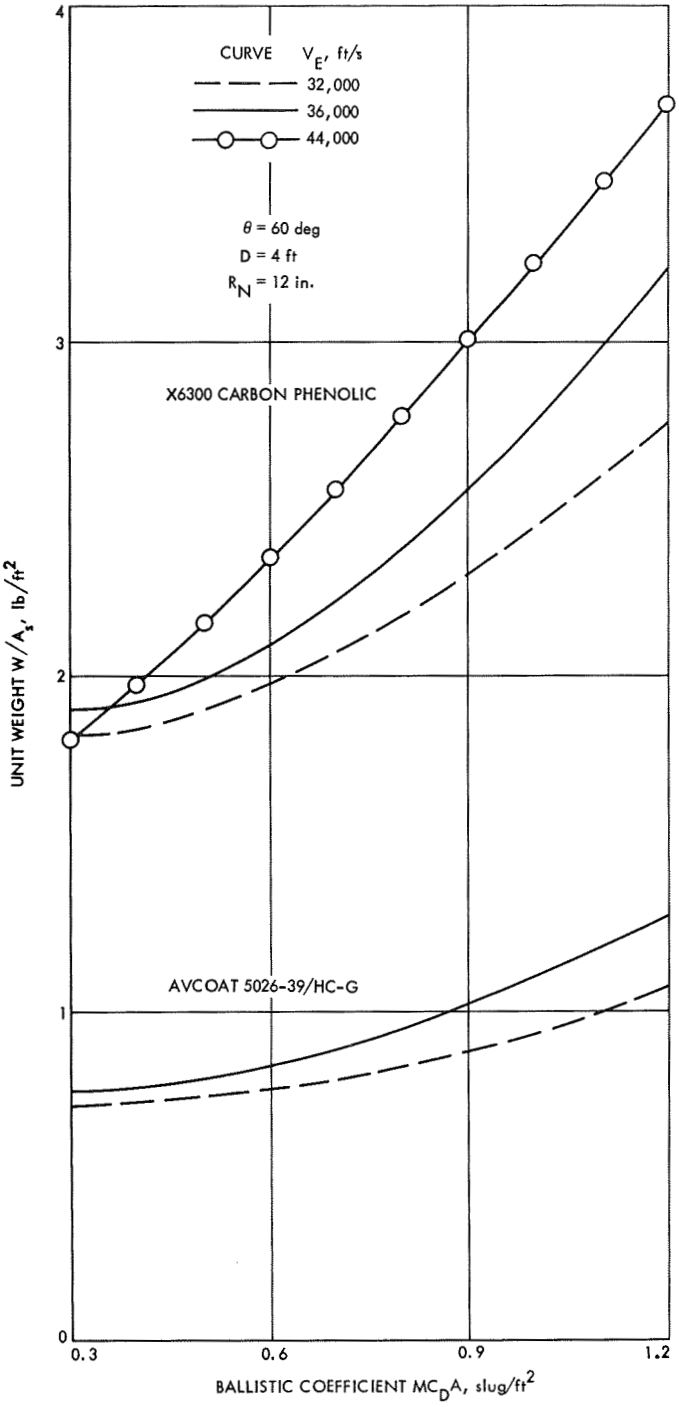

Fig. 23. Effect of ballistic coefficient on heat-shield unit weight, $\gamma_E = -45$ deg

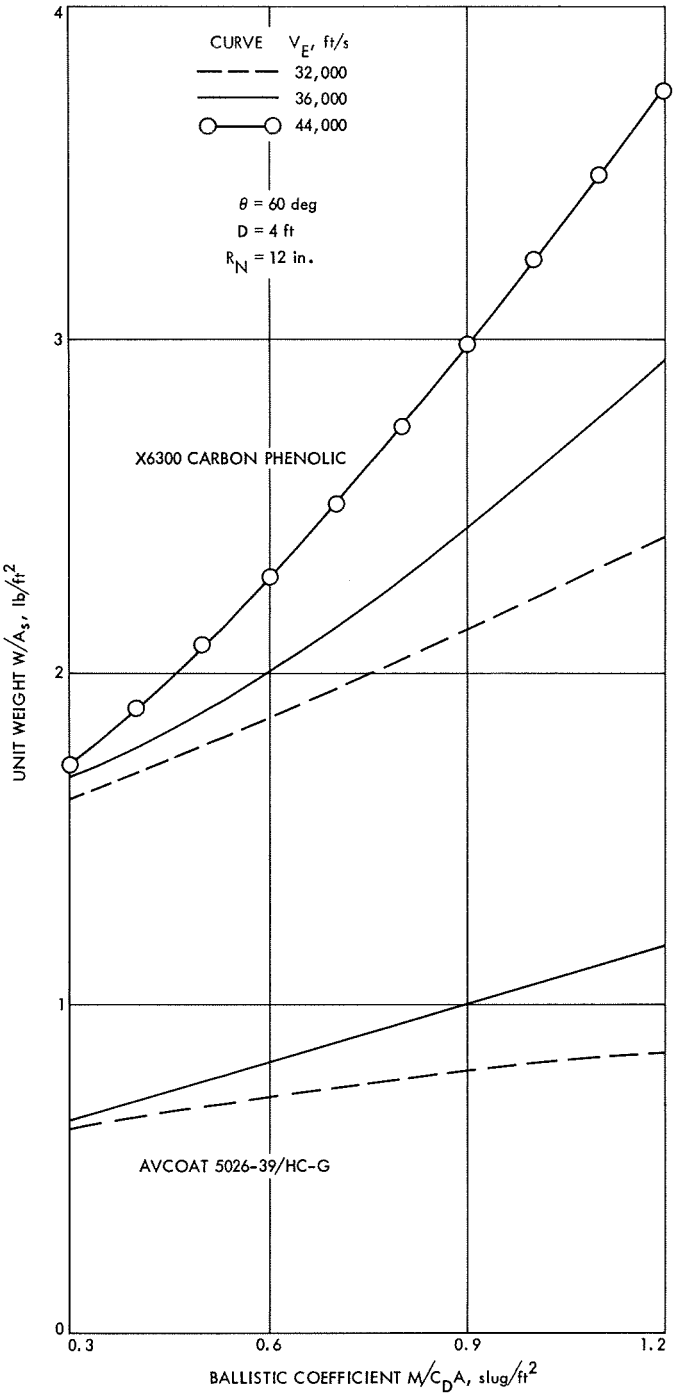

Fig. 24. Effect of ballistic coefficient on heat-shield unit weight, $\gamma_E = -90$ deg

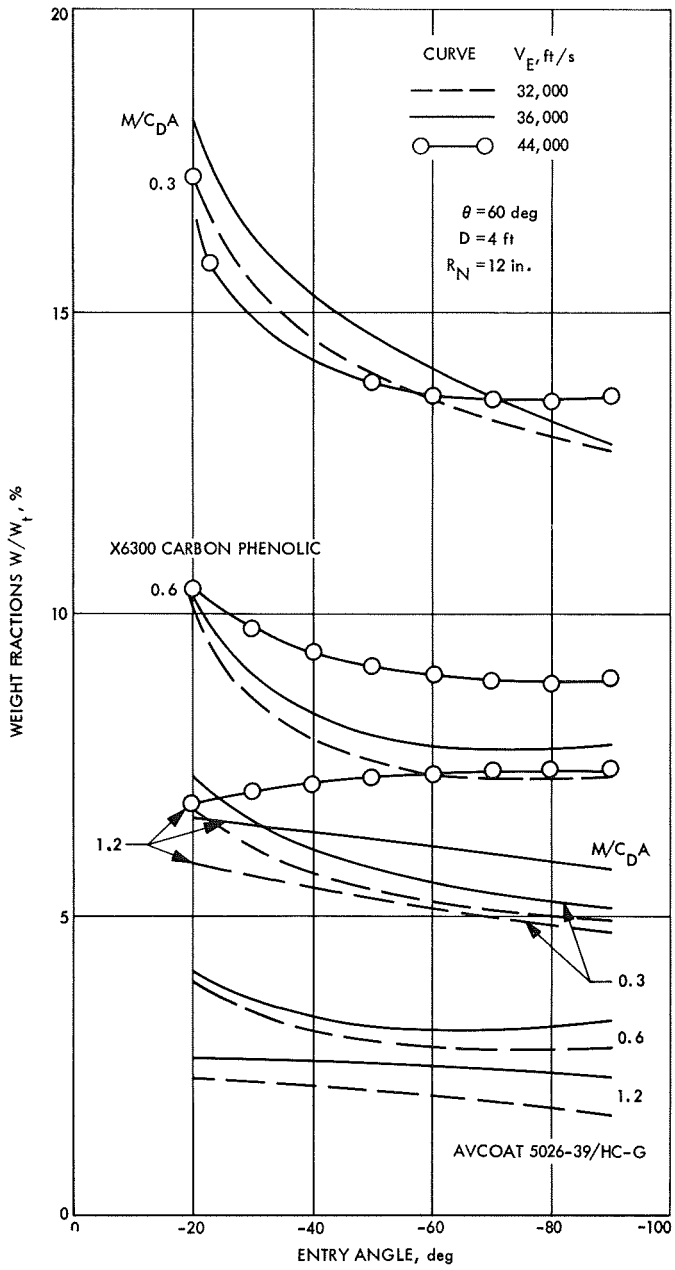

Fig. 25. Effect of entry angle on heat-shield weight fractions

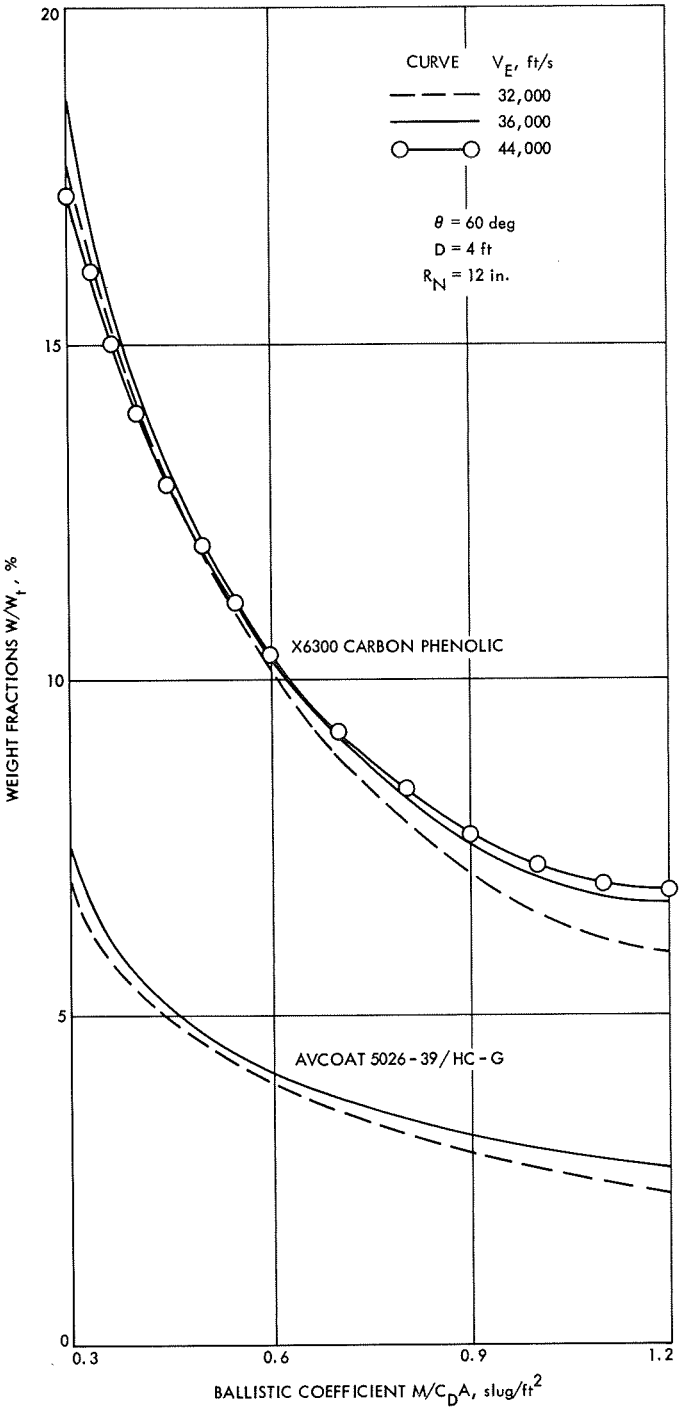

Fig. 26. Effect of ballistic coefficient on heat-shield weight fractions, $\gamma_E = -20$ deg

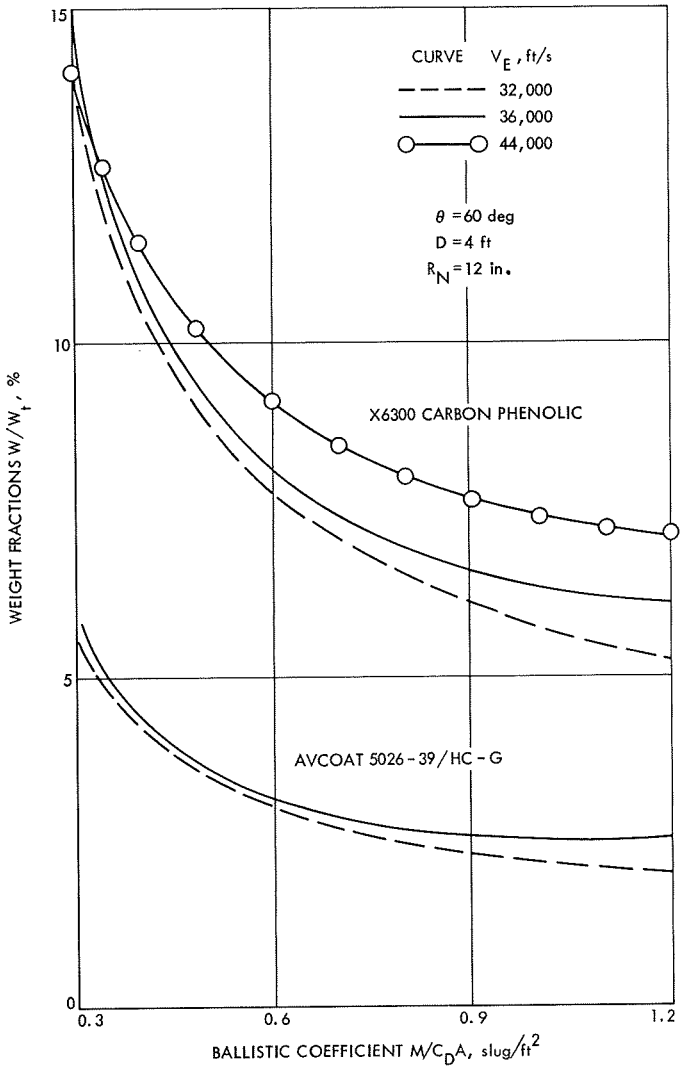

Fig. 27. Effect of ballistic coefficient on heat-shield weight fractions, $\gamma_E = -45$ deg

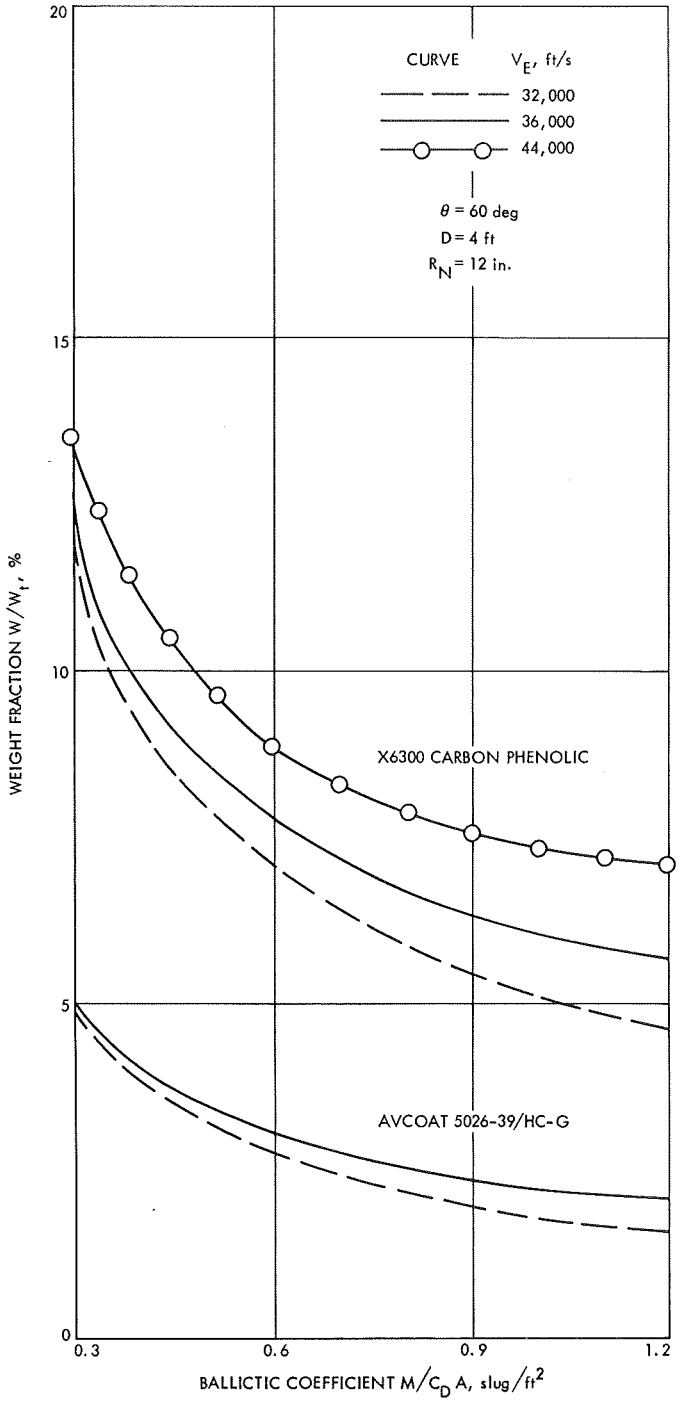

Fig. 28. Effect of ballistic coefficient on heat-shield weight fractions, $\gamma_E = -90$ deg

from the Avcoat curves to the carbon phenolic curves because of the pressure and shear conditions exceeding the mechanical strength of the lower density ablator. Figure 29 provides shear information that can be used to establish whether low- or high-density material should be used.

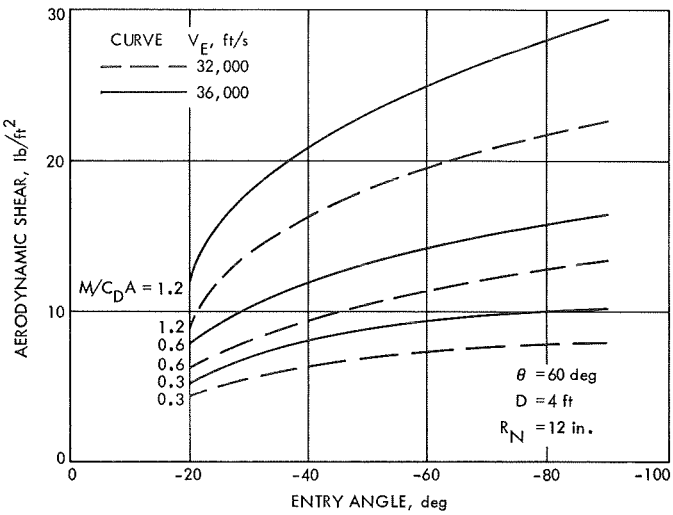

Fig. 29. Effect of entry angle on estimated aerodynamic shear

E. Comparison of Shape Alternatives

The heat-shield requirements for several variations in body diameter and nose radius are given in Table 8. Again, all values include the appropriate safety factor as discussed earlier. Plots for interpolation of these data are provided in Figs. 30 and 31. Heat-shield requirements appear to have only a weak dependence on base diameter. Figure 32 presents the effects of body shape on shear.

At the lower entry velocities where radiative heating effects are comparatively small, sharp-nose-radii vehicles require larger weight fractions of heat shield because of an accentuation of the importance of convective heating. As the velocity goes up, radiative heating increases at a faster rate and the larger nose radius become less desirable. The weight fraction for larger nose radii is larger for the 44,000-ft/s case.

All of the data up to this point have been for 60-deg half-cone angles. In Fig. 33 the effect of half-cone angle on heat-shield weight fractions is shown for nominal runs at entry velocities of 32,000 and 36,000 ft/s. A decreasing half-cone angle increases the heat-shield requirements considerably, so that at 30 deg the requirements are nearly 4 times larger than at 60 deg. This increase is primarily the result of the large increase in cone surface area for the same base diameter while the cone angle decreases. It is also strongly affected by an early onset of turbulence.

Table 8. Heat-shield dimensional and weight data for shape alternatives

Trajectory data						Avcoat 5026-39/HC-G					X6300 carbon phenolic				
Computer run	V_E, ft/s	M/C_DA, slug/ft^2	γ_E, deg	D, ft	R_N, in.	δ_0, in.	δ_j, in.	δ_{sh}, in.	W/A_s, lb/ft^2	W/W_t	δ_0, in.	δ_j, in.	δ_{sh}, in.	W/A_s, lb/ft^2	W/W_t
5	32,000	0.6	−45	4	12	0.280	0.278	0.290	0.77	0.030	0.263	0.262	0.272	1.97	0.077
10				4	4	0.330	0.309	0.304	0.82	0.032	0.311	0.290	0.284	2.09	0.082
11				2	12	0.287	0.278	0.308	0.77	0.030	0.270	0.262	0.287	1.98	0.077
12				2	4	0.330	0.309	0.311	0.81	0.032	0.311	0.290	0.291	2.08	0.082
13				8	12	0.288	0.278	0.308	0.82	0.032	0.271	0.262	0.292	2.11	0.083
14				8	4	0.333	0.309	0.312	0.84	0.033	0.314	0.290	0.291	2.15	0.085
19	36,000	0.6	−45	4	12	0.312	0.296	0.321	0.84	0.033	0.286	0.270	0.292	2.09	0.082
24				4	4	0.377	0.342	0.339	0.91	0.036	0.346	0.313	0.311	2.28	0.090
25				2	12	0.309	0.290	0.325	0.81	0.032	0.282	0.267	0.296	2.03	0.079
26				2	4	0.375	0.343	0.327	0.86	0.034	0.344	0.314	0.299	2.16	0.085
27				8	12	0.317	0.300	0.360	0.93	0.037	0.290	0.273	0.328	2.32	0.091
28				8	4	0.378	0.345	0.366	0.98	0.039	0.346	0.314	0.331	2.42	0.095
33	44,000	0.6	−45	4	12	—	—	—	—	—	0.443	0.271	0.340	2.36	0.093
38				4	4						0.344	0.268	0.336	2.33	0.092
39				2	12						0.457	0.275	0.343	2.37	0.092
40				2	4						0.343	0.267	0.334	2.25	0.088
41				8	12						0.462	0.275	0.345	2.43	0.095
42				8	4						0.344	0.270	0.336	2.38	0.094

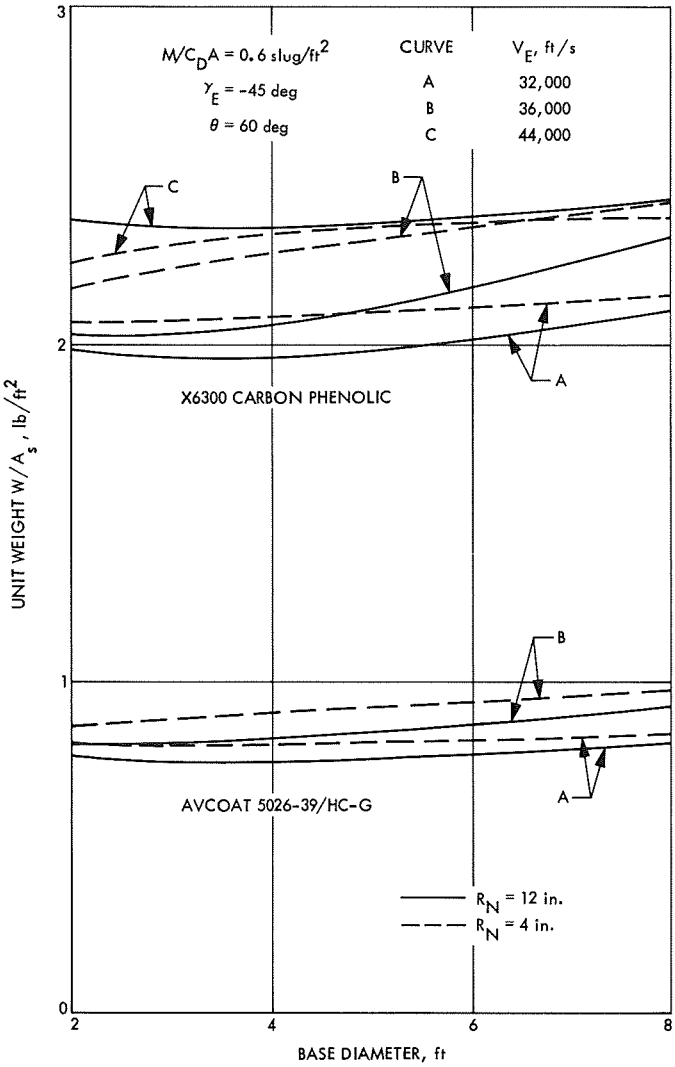

Fig. 30. Effect of body base diameter on heat-shield unit weight

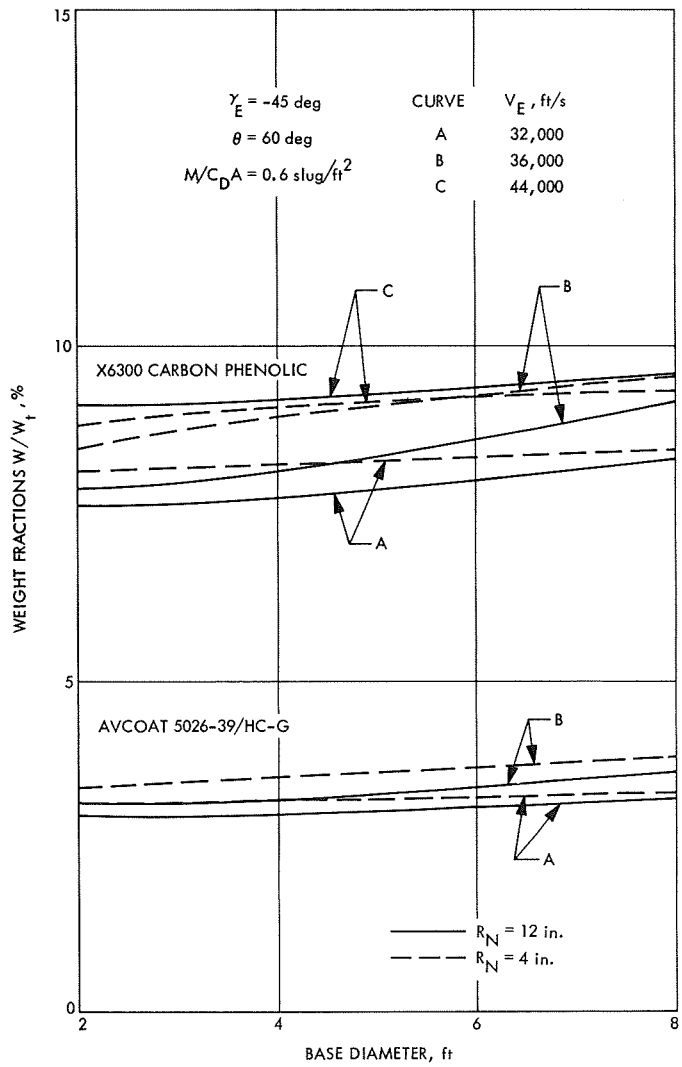

Fig. 31. Effect of body base diameter on heat-shield weight fractions

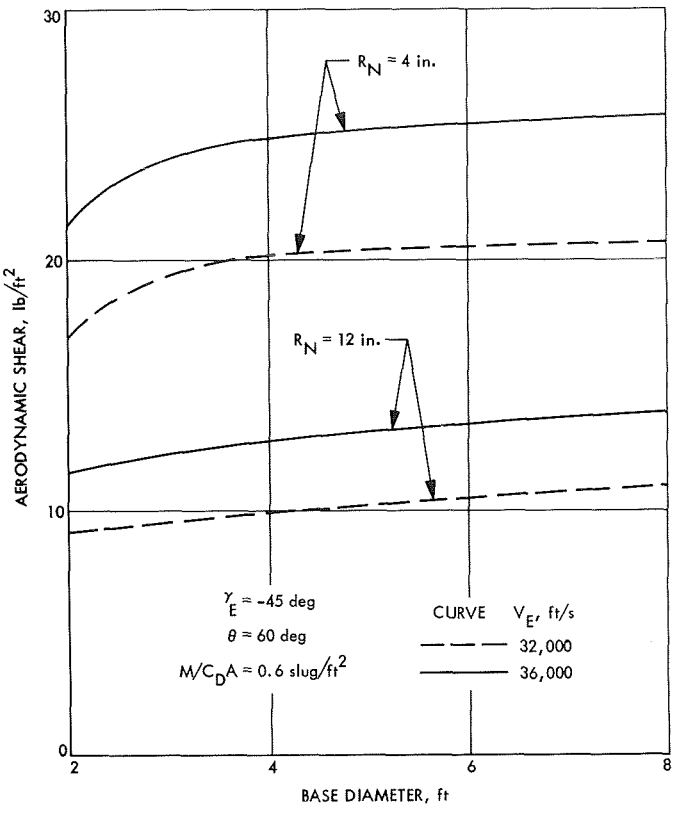

Fig. 32. Effect of body base diameter on estimated aerodynamic shear

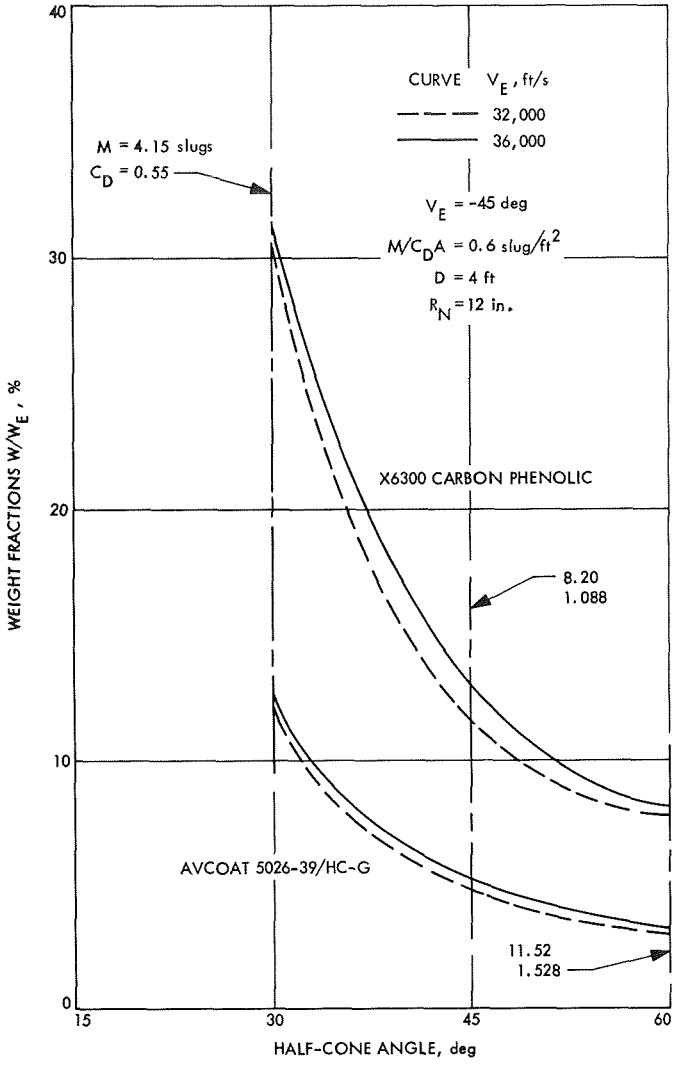

Fig. 33. Effect of half-cone angle on heat-shield weight fractions

The comparison in Fig. 33 is for the constant ballistic coefficient. Since drag coefficient decreases with a decrease of the half-cone angle, the mass of the vehicle for the same geometry must be changed to keep the ballistic coefficient at the same value. The numerical values, given on the curve at 30-, 45-, and 60-deg half-cone angles, represent the vehicle mass and the drag coefficient. If, on the other hand, vehicle mass remained constant, the ballistic coefficient would have to change. Thus, for 30- and 45-deg half-cone angles, the corresponding ballistic coefficients would be 1.67 and 0.845 slug/ft². In the latter case, the rate of mass fraction increases with a decrease in the half-cone angle at a somewhat slower rate than that shown in Fig. 33. However, the difference should not be substantial, as could be inferred from Fig. 27.

Another factor which might be included in this discussion is the need for heat shield on the rear portion of the vehicle to protect against wake heating. Since the shape of this aft cover is highly dependent on payload configuration design, this calculation was not included as part of this study. A detailed analysis should be made when a specific project mission is selected. In some studies this aft cover thermal protection is lumped with the aft cover structure to prevent confusion with the fore-body heat shield.

F. Structure Strength Considerations

During an atmospheric entry, vehicle structure will be subjected to external gas pressure and heating which primarily determine its in-flight strength requirements. Because the strength of structural material diminishes in varying degrees (depending on the material used) at elevated temperatures, the time-dependent pressure and temperature profiles, as applied to a structure, will therefore provide important information for stress analysis.

In the absence of substantial heating of the structure's back wall (which is normally the case) the maximum temperature that a structure will experience is the bond-line temperature (consideration of final descent is excluded). The magnitude of corresponding pressure and its distribution over the body in hypersonic flight can be approximately related to the dynamic pressure. Thus, time-dependent dynamic pressure and bond-line temperature profiles should represent adequate data for use in stress calculations for the structure.

Figure 34 is an example of entry at 36,000 ft/s, with a ballistic coefficient of 0.6 slug/ft^2, and three different entry angles. The dynamic pressure data were obtained from entry-trajectory computer runs and the bond-line temperature history from corresponding heat-shield performance calculations for Avcoat material. It is clear that in all cases the maximum bond-line temperature occurs almost at the end of entry time when the dynamic pressure has dropped to a negligible value.

Therefore, it would appear that, in general, temperature effects on structure should not be significant. However, the chart indicates that temperatures as high as 300°F (760°R) and dynamic pressures near 1300 lb/ft^2 (9 psi) can be expected to occur simultaneously in this particular case, and such a situation may have to be taken into account, especially when a structure built of plastic composite material is contemplated.

VI. Simulation Capabilities

Standard procedures for any entry mission normally entail some form of ground or flight "proof-test" to verify the design and ensure reliability. For the Venus missions generally under consideration, there are difficulties inherent in both ground-simulation and earth-flight tests. Starting with the heating-time histories shown in Fig. 7, certain observations can be made as to the existing simulation capabilities.

A. Ground Simulation

Ground simulation is never fully satisfactory for any mission because convective heating, radiative heating, enthalpy, pressure, and gas composition are difficult to simulate all at once on a single sample. Even where full simulation is possible, the transient nature of the environment makes it impossible to follow the full pulse in one experimental setup. In standard practice, analysis implies which environmental constraints have the smallest effect on heat-shield performance, then only partial simulations are made incorporating all important phenomena in separate but related tests.

Most of the ground simulation of entry at NASA is accomplished in extensive plasma-arc facilities at Ames Research Center (ARC), Langley Research Center (LaRC), and Manned Spacecraft Center (MSC). A chart of the NASA ground-simulation capability for Venus entry is shown in Fig. 35 with the convective heating-pressure histories of the four nominal cases. A more complete description of the facilities involved is provided in Ref. 30. All specimen sizes are limited to 1.25-in. diam to provide a compromise between the highest obtainable heating rates and the smallest specimen size for which the lateral heating effects do not invalidate the ablation data based on centerline recession rates.

The important item to derive from this chart is that the lower velocity missions are adequately simulated by the existing capability, including the fact that ARC can presently superimpose 1000 Btu/ft^{2}s of radiative heating (on a 1-in. sample) over the convective heating test, and MSC can superimpose 500 Btu/ft^{2}s. The 40,000-ft/s mission is borderline and, although it cannot be fully simulated, it is probably within the range of reasonable extrapolation. The Venus–Mercury flyby with a probe mission at 44,000 ft/s is outside the bounds of present test capability, especially in relation to the 13,121 Btu/ft^{2}s of radiant heating under peak conditions. There is some effort toward providing higher-rate radiant heating facilities to alleviate this testing problem but it is unlikely that timing will allow early utilization. Even for the missions that can be simulated, the test facilities are supplements to analysis rather than to proof tests.

B. Earth Flight Test

Simulation of Venus atmospheric entry by a earth reentry flight test has been extensively covered by Spiegel, Wolf, and Zeh in Ref. 14. Based on their efforts, a 90-deg entry into earth atmosphere at the same velocity and ballistic coefficient appears to adequately simulate the deceleration, angle of attack envelope, and heat-shield response of Venus entry at a 45-deg-path angle in spite of large differences in gas composition. Since most of the ablation rate is controlled by sublimation or evolved species chemical erosion, combustion-process differences in air or CO_2 mixtures have little effect. The higher radiation load anticipated for CO_2 atmospheres also did not appear to give an equivalent response when integrated into material performance. Based on this type of information, an earth proof-test for low-angle Venus entry (less than 45 deg)

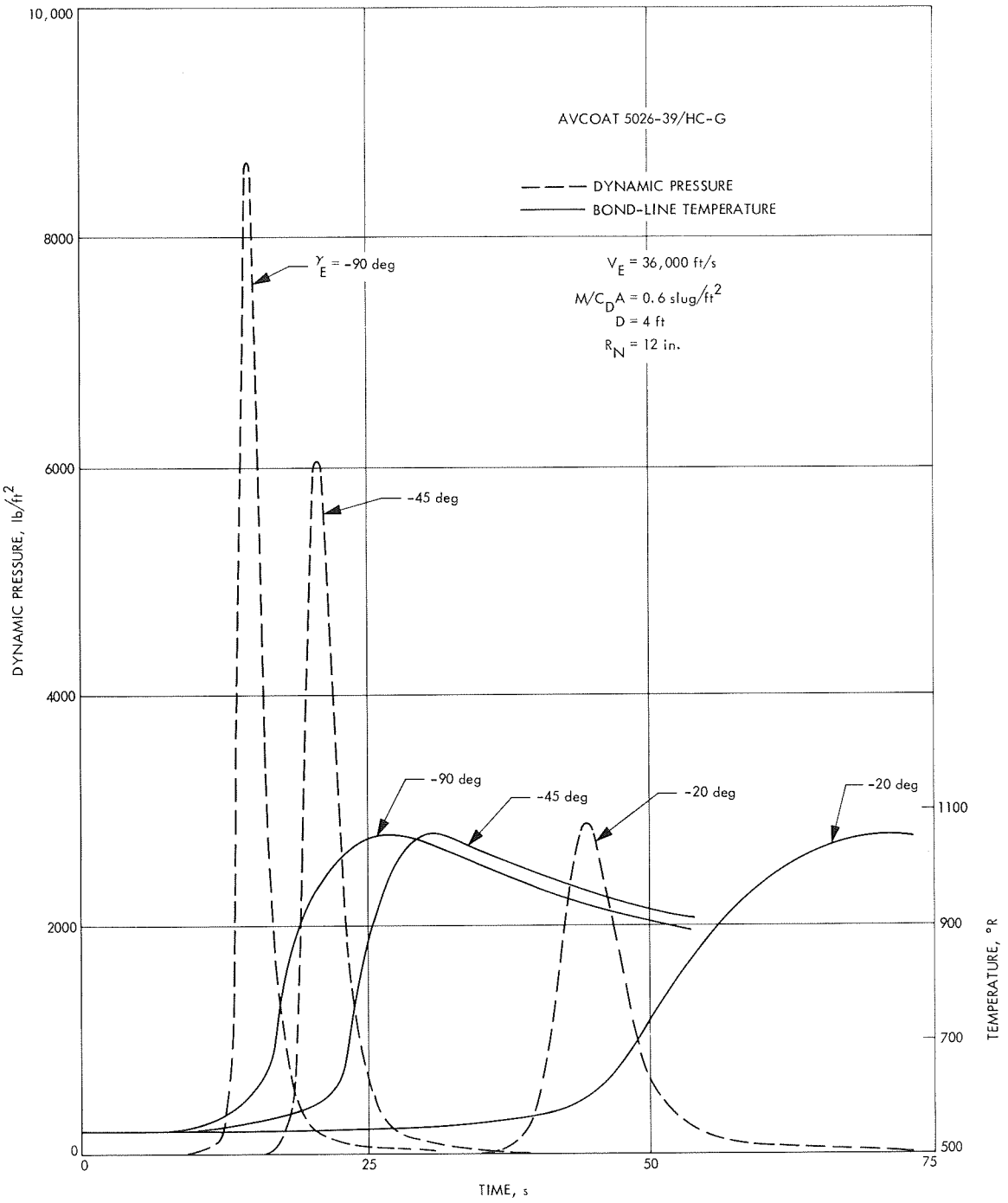

Fig. 34. Dynamic pressure and bond-line temperature

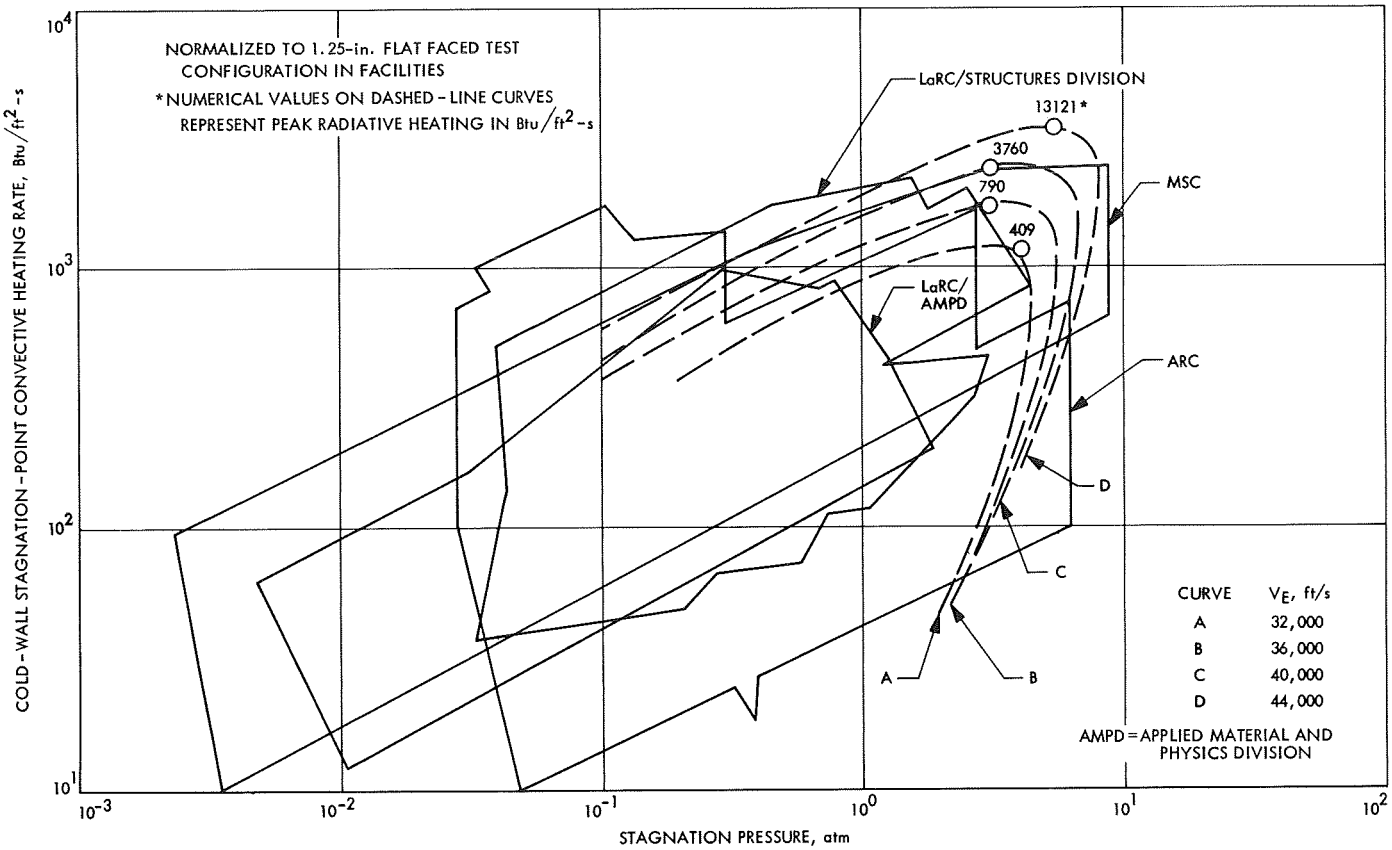

Fig. 35. NASA ground test simulation capability in relation to typical Venus trajectories

could be designed that would verify heat-shield performance in a conservative sense in which the presence of unknown sources of catastrophic failure could be eliminated. Extrapolation of these conclusions based on a 36,000-ft/s-entry-velocity analysis to the 44,000-ft/s case must be checked in view of higher radiative heating levels.

VII. Projected Needs

Before the results are summarized, a review of the major limitations in the analysis and of the recommendation regarding directions of attack to improve these limitations is warranted. The major areas for improvement are in the mathematical models for analysis, in the sources of input data for analysis, and in the simulation facilities necessary to integrate environmental effects for verifying analysis.

The analysis techniques incorporated in the computer programs described in this report, including one adopted for the present study, are not completely adequate to handle entries with very high convective and radiative heat loads. A case in point, for example, would be the process of sublimation and its interaction with internal decomposition. Furthermore, additional refinements in the numerical techniques and controls are also desirable to enable a stable solution, particularly at high-surface recession rates when the front surface overtakes the degradation zone. Sublimation of char remains a problem, and more theoretical as well as experimental research is required to establish a satisfactory mathematical formulation of the process. Other analytical areas needing extensive additional work are the effects of combustion in the boundary layer, absorption of shock layer radiation by evolved carbon species, chemical erosion of high-temperature surface carbon by evolved gases percolating up through the char, shear in high ablation rates, and a char conductance model as a function of heat treatment. A number of preliminary efforts have been initiated in many of these areas, but generally verified models are not yet available. Some of the more recent efforts related to these aspects are reported in Refs. 31–33.

The available heat-shield materials appear to be adequate for Venus entry missions studied in this report; however, some effort should be made to improve the resistance to shear, especially in the materials of lower

density. The most difficult problem experienced at the present time is the lack of information on some of the material properties required for heat-shield performance analysis. In this area, a comprehensive program should be instituted to fill these needs.

Finally, the means of ground simulation should be further developed and perhaps new ways of simulation, using novel high-energy heat sources, should be seriously explored. As mentioned earlier, very high radiative fluxes at velocities above 36,000 ft/s combined with high convective heat loads, high pressures, and high shear make the presently available ground simulation facilities incapable of adequate simulation.

VIII. Summary

In the foregoing analysis the heat-shield requirements for a likely range of possible Venus entries have been computed considering typical charring ablators. The data obtained were presented in tabular and graphical form for general utilization. Some difficulties have been encountered in the process mainly because of the inadequacy of the available computer programs and the lack of accurate information of thermo-ablation properties of materials. These problems have introduced uncertainties that had to be carefully evaluated.

Based on the most probable Venus atmosphere, as derived from the data obtained from the flyby and penetrating probes as well as radar, the thermal environments have been determined for a matrix of cases covering the entry velocity range of 32,000 to 44,000 ft/s. Here, too, considerable uncertainties had to be recognized in the calculation of convective and radiative heat transfers. These uncertainties have been combined with those indicated above by means of error analysis to obtain overall uncertainty factors.

For two basic materials used in the analysis, the maximum probable uncertainty factors were determined to be just below 1.5. However, when materials substantially different in thermo-ablation properties are considered, these uncertainties should be reevaluated to insure safety of the heat-shield design.

The available heat-shield materials were found to satisfactorily meet the requirements of Venus entries, provided their compatibility with the degree of heat and shear-load severity is ascertained in each case. In this respect, lower density materials should perform satisfactorily for entry velocities up to 36,000 ft/s and lower ballistic coefficients. For higher energy entries, denser materials with better resistance to thermal and shear erosions should be used.

With regard to vehicle shape, half-cone angle is shown to have the strongest influence on heat-shield performance, and heat-shield weight increases markedly with a decrease in this angle. The combined effects of base diameter and nose radius, on the other hand, affect heat-shield weight to a much lesser degree.

Considerable effort is still needed in the following three areas listed here in order of their importance, namely: (1) the accurate determination of thermo-ablation properties (through adequate testing) for applicable heat-shield materials, (2) the development of a ground simulation facility covering the required testing range for Venus entries, and (3) the improvement of analysis techniques. With these tasks accomplished, closer prediction of heat-shield requirements will be possible.

Nomenclature

A circular area corresponding to diameter D, ft²

A_s total surface of heat shield, ft²

A_0 area at stagnation point, ft²

$\overline{B}$ correction factor for carbon vapor recondensation

C_D drag coefficient

c_p local material specific heat, Btu/lb-°R

c_{p_c} specific heat of char, Btu/lb-°R

c_{p_v} specific heat of virgin material, Btu/lb-°R

D body base diameter, ft

H enthalpy, Btu/lb

k local material thermal conductivity, Btu/h-ft-°R

k_c thermal conductivity of char, Btu/h-ft-°R

k_v thermal conductivity of virgin material, Btu/h-lb-°R

M vehicle mass, slug

M_0 molecular weight at standard conditions, lb/lb mole

$\dot{m}$ virgin material decomposition rate, lb/ft²-h

P_E entry spin rate, rad/s

p pressure, lb/ft²

p_0 pressure at stagnation point, lb/ft²

$\dot{q}_c$ convective heat flux, Btu/ft²-s

$\dot{q}_{c_0}$ convective heat flux at stagnation point, Btu/ft²-s

$\dot{q}_r$ radiative heat flux, Btu/ft²-s

R_0 gas constant, Btu/lb mole-°R

R body radius, ft

R_N nose radius, ft (in.)

r_c specific heat density function

r_k thermal conductivity density function

S distance from stagnation point along body contour, ft

s surface recession, in.

$\dot{s}_s$ surface recession rate due to sublimation, ft/s

T_0 reference temperature (492°R), °R

T_s surface temperature, °R

V flight velocity, ft/s

V_E entry velocity, ft/s

W heat shield weight, lb

W_t total weight of entry vehicle, lb

α_E angle of attack at entry

β' sublimation rate coefficient, ft/s-°R

β'' order of reaction for sublimation

β''' activation temperature for sublimation, °R

γ_E entry angle, deg

δ_0 stagnation point heat-shield thickness, in.

δ_j heat shield thickness at the junction, in.

δ_{sh} heat shield thickness at the shoulder, in.

$\Delta\delta$ maximum probable deviation in heat shield thickness, in.

ϵ surface emittance

θ half-cone angle, deg

ρ local material density, lb/ft³

ρ_c char density, lb/ft³

ρ_v virgin material density, lb/ft³

Subscripts

n nominal value

References

1. Nagler, R. G., "Tailoring Polymers for Entry Into the Atmospheres of Mars and Venus," *J. Macromol. Sci.–Chem.*, Vol. A3, No. 4, pp. 763–802, July 1969.

2. *Mars–Venus Capsule Parametric Study: Volume III. Venus Results,* Final Report on JPL Contract 950626. Avco Corporation, New York, Jan. 16, 1964.

3. Katz, G. D., and McMullen, J. C., "Entry Vehicles for Unmanned Planetary Exploration," in *AIAA Publication CP-9,* proceedings of the AIAA Entry Technology Conference, held in Williamsburg, Va., Oct. 12–14, 1964. General Electric Company, Philadelphia, Pa.

4. Bourke, R. D., et al., "First Generation Lander for the 1973 Venus Opportunity," Paper 68-156, presented at the Sixth Aerospace Sciences Meeting, New York, Jan. 22–24, 1968.

5. *Venus Flyby/Entry Probe Mission Study, 1972,* Final Report on JPL Contract 951964. Avco Corporation, Space Systems Division, Lowell, Mass., Apr. 1968.

6. Florence, D. E., *Aerothermodynamic Considerations of a Venus Entry Probe,* Report TIS 68SD 438. General Electric Company, Philadelphia, Pa., Apr. 1968.

7. Ducsai, S. J., et al., *Planetary Systems–Venus Probe Study,* Final Report. Martin Marietta Corporation, Denver, Colo., June 6, 1968.

8. *Buoyant Venus Station Feasibility Study: Volumes I-VI.* Final Report. Martin Marietta Corporation, Denver, Colo., 1967.

9. *A Venus Multiple-Entry-Probe Direct-Impact Mission, Scientific Objectives and Technical Description,* Goddard Space Flight Center, Greenbelt, Md., Jan. 1969.

10. Eckman, P. E., *Mariner Venus/Mercury 1973 Study,* Technical Memorandum 33-434. Jet Propulsion Laboratory, Pasadena, Calif., Aug. 1, 1969.

11. *Models of Venus Atmosphere, 1968,* NASA SP-8011. National Aeronautics and Space Administration, Washington, D.C., Dec. 1968.

12. Horton, T. E., *The JPL Thermochemistry and Normal Shock Computer Program,* Technical Report 32-660. Jet Propulsion Laboratory, Pasadena, Calif., Nov. 1, 1964.

13. *JPL Entry Vehicle Design Computer Program Users' Manual,* prepared on JPL Contract 951070. Avco Corporation, Lowell, Mass., May 26, 1966.

14. Spiegel, J. M., Wolf, F., and Zeh, D. W., "Simulation of Venus Atmospheric Entry by Earth Reentry," Paper 68-1148, presented at the AIAA Entry Vehicle Systems and Technology Meeting, Williamsburg, Va., Dec. 3–5, 1968.

15. Page, W. A., et al., "Radiative Transport in Inviscid Nonadiabatic Stagnation-Region Shock Layers," Paper 68-784, presented at the Third AIAA Thermophysics Conference, Los Angeles, Calif., June 24–26, 1968.

16. Brunner, M. J., "Analysis of the Aerodynamic Heating for a Reentrant Space Vehicle, *Trans. ASME, Ser. C: J. Heat Transfer,* p. 223, Aug. 1959.

References (contd)

17. Livingston, F., and Williard, J., "Planetary Entry Body Heating Rate Measurements in Air and Venus Atmospheric Gas up to T = 15,000°K," Paper 69-635, presented at the Fourth Thermophysics Conference, San Francisco, Calif., June 16–18, 1969.

18. Wolf, F., and Spiegel, J. M., "Status of Basic Shock-Layer Radiation Information for Inner-Planet Atmospheric Entry, *J. Spacecraft Rockets*, Vol. 4, No. 9, pp. 1166–1173, Sept. 1967. Also available as Technical Report 32-1195. Jet Propulsion Laboratory, Pasadena, Calif., 1967.

19. Swann, R. T., Pittman, C. M., and Smith, J. C., *One-Dimensional Numerical Analysis of the Transient Response of Thermal Protection Systems*, NASA TH-D-2976. National Aeronautics and Space Administration, Washington, D.C., Sept. 1965.

20. Stroud, C. W., *A Study of the Reaction-Plane Approximation in Ablation Analysis*, NASA TN-D-4817. National Aeronautics and Space Administration, Washington, D. C., Oct. 1968.

21. Curry, D. M., *An Analysis of a Charring Ablation Thermal Protection System*, NASA TN-D-3150. National Aeronautics and Space Administration, Washington, D.C., Dec. 1965.

22. *An Advanced Analytical Program for Charring Ablators: Volumes I and II.* Final Report on NASA Contract NAS 9-4329. Avco Corporation, Space Systems Division, Lowell, Mass., 1967.

23. "Aerotherm Equilibrium Surface Thermochemistry Program," *Users' Manual*, Version 2. Aerotherm Corporation, Mountain View, Calif., Jan. 1966.

24. "Aerotherm Charring Material Ablation Program," *Users' Manual*, Version 2. Aerotherm Corporation, Mountain View, Calif., Jan. 1966.

25. Price, R. E., and Schultz, F. E., *Modification of the One-Dimensional REKAP Program to Allow for Charring in Three Material Layers*, NACA CR-72488. National Aeronautics and Space Administration, Washington, D.C., Jan. 2, 1969.

26. Dolton, T. A., et al., "Thermodynamic Performance of Carbon in Hyperthermal Environments," Paper 68-754, presented at the Third AIAA Thermophysics Conference, Los Angeles, Calif., June 24–26, 1968.

27. Bishop, W. M., and DeCristina, V., "The Combustion and Sublimation of Carbon at Elevated Temperatures, "Paper 68-759, presented at the Third AIAA Thermophysics Conference, Los Angeles, Calif., June 24–26, 1968.

28. Zavitsanos, P. C., *The Vaporization of Pyrolytic Graphite*, prepared for U.S. Air Force Ballistic System Division on Contract AF 04 (694)-222. General Electric Company, Missile and Space Division, Philadelphia, Pa., May 1966.

29. Beers, Y., *Introduction to the Theory of Error.* Addison–Wesley Publishing Co., Inc., Reading, Mass., 1958.

30. Nagler, R. G., *A Systematic Review of Heat-Shield Technology for Extraterrestrial Atmospheric Entry*, Technical Report 32-1436. Jet Propulsion Laboratory, Pasadena, Calif. (in press).

References (contd)

31. Kendall, R. M., et al., "A Multicomponent Boundary Layer Chemically Coupled to an Ablating Surface," *AIAA J.*, Vol. 5, No. 6, pp. 1063–1071, June 1967.

32. Woodruff, L. W., and Lorenz, G. C., "Hypersonic Turbulent Transpiration Cooling Including Downstream Effects," *AIAA J.*, Vol. 4, No. 6, pp. 969–975, June 1966.

33. Nagler, R. G., "The Thermal Conduction Process in Carbonaceous Chars," in *Proceedings of the Sixth Conference on Thermal Conduction, Dayton, Ohio, October 19–21, 1966.* Also available as Technical Report 32-1010. Jet Propulsion Laboratory, Pasadena, Calif., Feb. 1967.

NASA — JPL — Coml., L.A., Calif.